This is the Pre-Published Version.

This version of the article has been accepted for publication, after peer review (when applicable) and is subject to Springer Nature's AM terms of use (https://www.springernature.com/gp/open-research/policies/accepted-manuscript-terms), but is not the Version of Record and does not reflect post-acceptance improvements, or any corrections. The Version of Record is available online at: http://dx.doi.org/10.1007/s41061-024-00458-9.

Water soluble small organic fluorophores for oncological theragnostic applications: Progress and development

Ashanul Haque[1,2*], Khalaf M. Alenezi,[1, 2] Abdulmohsen Khalaf Dhahi Alsukaibi,[1, 2] Ahmed A. Al-Otaibi,[1, 2] Wai-Yeung Wong[3,*]

[1] Department of Chemistry, College of Science, University of Ha'il, Ha'il 81451, Saudi Arabia.

[2] Medical and Diagnostic Research Centre, University of Ha'il, Ha'il 55473, Saudi Arabia.

[3] Department of Applied Biology and Chemical Technology, The Hong Kong Polytechnic University, Hung Hom, Kowloon, Hong Kong, P. R. China.

Correspondence: a.haque@uoh.edu.sa (AH); wai-yeung.wong@polyu.edu.hk (WYW)

Abstract

Cancer is one of the major non-communicable diseases responsible for millions of deaths every year worldwide. Though various cancer detection and treatment modalities are available today, many deaths occur due to its late-stage detection and the metastatic nature. Noninvasive detection using luminescence-based imaging tools is considered one of the promising techniques due to its low cost, high sensitivity, and brightness. Moreover, these tools are unique and valuable as they can detect even the slightest changes in the cellular microenvironment. To achieve this, a fluorescent probe with strong tumour uptake and high spatial and temporal resolution, especially water-soluble, is highly demanded. Recently, several water-soluble molecules with emission windows in visible (400–700 nm), first near-infrared (NIR-I, 700–1000 nm) and second near-infrared (NIR-II, 1000–1700 nm) windows, have been reported in the literature. This review highlights recently reported water-soluble small organic fluorophores/dyes with applications in cancer diagnosis and therapeutics. We systematically highlighted and uncovered the key concepts, structural classes of fluorophores, strategies for imparting water solubility, and applications in cancer therapy and diagnosis, i.e., theragnostic. We discussed examples of water-soluble fluorescent probes based on coumarin, xanthene, boron–dipyrromethene (BODIPY) and cyanine cores. Some other emerging classes of dyes based on carbocyclic and heterocyclic cores have also been discussed. Besides, emerging molecular engineering methods to obtain such fluorophores have been discussed. Finally, the opportunities and challenges in this research area have also been delineated.

Keywords: Applications; Cancer; Diagnostics; Fluorophores; Imaging; Water soluble; Therapeutics.

1. Introduction

Cancer, defined as a group of non-communicable diseases, is one of the major causes of mortality and morbidity worldwide. In 2020 alone, more than 19 million cancer patients have been detected, with ~ 10 million deaths.[1] According to a report, this number would increase soon and add hundreds of billions of dollars to the burden on the economy.[2] The best strategy to improve the mortality/ morbidity rate is to detect cancer in its earlier stage. To this end, traditional modalities, including computed tomography (CT), planar scintigraphy, positron emission tomography (PET), single photon emission computed tomography (SPECT), magnetic resonance imaging (MRI), and ultrasound (US) are available.[3] These diagnostic techniques offer unique advantages and disadvantages. For example, MRI is a powerful, non-invasive imaging technology that requires contrast agents, mostly heavy metal-containing compounds.[4] However, in many ways, these agents are still primitive, with no molecular selectivity, short clearance times, renal toxicity, and low sensitivity offered by probes. Furthermore, repeated measurement is carried out to compensate for the low signal intensity, which causes long imaging times and makes MRI technique quite expensive. Often, these are used in combination to achieve the maximum effect.[5] Similarly, the problems of insufficient sensitivity, low resolution and poor signal-to-background ratio (SBR) remain a significant challenge.

Non-invasive cancer detection using optical imaging (OI) techniques is gaining attention and popularity in biological and medical sciences.[6] Owing to its low cost, easy operation, fast response, high sensitivity, and non-invasive nature, OI techniques have gained worldwide interest.[5] Apart from the instrumental modules, a critical component of this technique is the probe/dye. A probe is a molecule/macromolecule used to label cells or genes and allow rapid and sensitive detection of abnormalities/upregulated analytes. An ideal probe should have excellent photophysical (such as long and intense emission with large Stokes-shift) and physicochemical properties (e.g., balanced lipophilicity-hydrophilicity character, small size, etc.), long circulation/retention time, high tumour uptake with no toxicity. Furthermore, they ought to be uncomplicated to synthesize and reproduce. Numerous organic, inorganic, nanoparticle, and hybrid systems have been investigated in the quest of such probes.[7] Although organic systems show inferior PL properties than organometallic, inorganic, and nano-based probes, they have gained research interest due to their tunable emission, good photostability, low toxicity, and non-radioactive nature.[8] The fact that organic probes are made up of a π-conjugated structure, they show strong light-trapping ability (absorption coefficient, ε), sufficient/reasonable quantum yield (Φ) and high molecular brightness (MB = ε × Φ) making them suitable for the imaging applications. Moreover, the targetability or specificity of a particular site could also be achieved by attaching a

suitable recognition/charged moiety. To date, numerous review articles have been dedicated to the exploration of fluorescent organic probes, including water-soluble small molecules and oligo/polymers.[9] In 2014, Fan, Yang and Chen [10] reviewed the application of a specific class (BODIPY and aza-BODIPY) of water-soluble synthetic dyes. Before this, Zhu and coworkers [11] highlighted the diagnostic and therapeutic applications of water-soluble conjugated polymers. At the same time, Li, Gao and Ma [9b] presented a comprehensive review of water-soluble chromo- and fluorogens. Sun and Schanze [12] recently reviewed protein sensing, flow cytometry labelling, and cancer therapy applications of various water-soluble conjugated polymers. Despite this, there is a lack of systematic literature on the application of water-soluble visible/NIR/FIR emitting single molecular entities with application in tumor diagnosis and therapy. To fill this gap, we present a comprehensive review summarising recent advances in water-soluble small organic fluorophores for cancer therapy. We covered key concepts, structural classes of fluorophores, strategies for imparting water solubility, and applications in cancer diagnosis and therapy. However, papers reported in the last five years are central to this review; some old but essential work has also been included in the discussion. Water soluble imaging probes based on the concept of supramolecular/nano-assemblies, formulations (emulsion, dots,), etc., are out of the scope of this review; however, few examples of nanoprobes based on NIR-II emitting fluorophores have been included.

2. Lipophilicity-hydrophilicity-emission balance: A challenge

In drug discovery, realizing a molecule/drug with high solubility in water, thus enhanced bioavailability, is an essential factor behind its success or failure.[13] This is incredibly challenging for the newly identified complex and large molecular weight molecules. Water solubility (hydrophilicity) is also an essential physico-chemical property for the dyes, whether it is developed for parental/oral delivery. While liposolubility is vital for cell permeability/penetration, hydrophilicity facilitates delivery and subsequent interaction with the pharmacological target.[14]These factors (liposolublity and hydrophilicity) are inversely related; therefore, maintaining balance without affecting emission features is a big challenge. Even though numerous state-of-the-art π-conjugated small molecules, oligomeric, and polymeric fluorescent probes with narrow emission bands and diverse imaging windows (visible to NIR-I/II regions) are available, poor aqueous solubility hinders their clinical applications. From the structural point of view, fluorophore contains a high degree of conjugation, which makes it hydrophobic. Besides, π–π stacking mediated aggregation in polar solvent leads to weak/quenched fluorescence. [15] To avoid these issues, high concentrations (>10%, v/v) of organic solvents are often used in place of real aqueous

environments, which can cause significant harm to living beings. Besides, photo-bleaching and fluorescence quenching of organic fluorophores, especially red-emitting probes, in aqueous and alcoholic media is also challenging.[16] In these probes quenching takes place through space by resonant energy transfer from the electronically excited dye to the combination bands of O–H vibrations in the (**Fig. 1a**).

To realize a water-soluble formulation suitable for clinical applications, chemical or physical strategies are adopted (Fig. 1b). Chemical manipulation includes installing one or more neutral or polar functional groups on the probe. Neutral groups containing electronegative atoms, such as oxygen or nitrogen, enhance the propensity of a probe towards water. In the case of charged groups, both cationic and anionic fragments are used. It is to be noted that in such cases, counterion also plays an important role. For example, a probe with bromide anion was more soluble than the one with acetate anion.[17] Charged side chains assist in H-bond formation with the environment (solvent) and attenuate intermolecular π–π aggregation of dyes due to steric/electrostatic factors leading to enhanced solubility.[15b, 18] Sulfonic acid groups over hydrophobic molecules shield the hydrophobic core and increase its solubility.[19] In the case of acidic/basic compound, formation of the corresponding salt is the most straightforward technique to improve its solubility. It was noted that a simple salt (e.g. hydrochloride) formulation is enough to impart solubility to phthalocyanine-based photodynamic therapy (PDT) agent than quaternization of nitrogen atoms.[20] Recently, Yanai et al.[18b] proposed a unique two-step approach to realize water-soluble BODIPYs incorporating (trifluoromethyl)sulfonyl stabilized carbanionic group. Not only did this method yield water-soluble and stable BODIPYs, but it also yielded new fluorescein and aminocoumarin derivatives. Another exciting aspect of this approach is that it converts hydrophobic BODIPYs resistant to sulfonylation reaction (3,5-dialkenyl-8-phenyl BODIPY) and tolerates a range of functionalities. However, a major drawback with chemical manipulation is the possible loss of activity in in-vivo models. Besides, not all compounds are compatible with such chemical modifications. When chemical modification is not feasible/possible on an organic fluorophore, it is converted to nano-assembly (e.g. PEGylation, self-assembly with the amphiphilic polymeric matrix, hydrophilic complex with a biomolecule etc.) to retain the solubility, emission properties and in some cases promotes cellular uptake. [16, 21] All NIR-II imaging probes are reported as nano-formulations in the literature. Most papers dealing with such probes also use one or more surfactants to prevent aggregation in physiological conditions.[22] This includes SDS (sodium dodecyl sulfate), Triton X-100 or Tween 10, CrEL, DMEM, etc.

Despite these options, existing solubilization strategies have various issues/challenges. For example, some dyes show additive-dependent emission.[23] It has also been noted that

some probes show different behavior in plasma and PBS.[24] In addition to this, long-term biosafety, molecular leakage and aggregation-caused fluorescence quenching of nanomaterials, tedious preparation and purification of the probe with a charged or neutral polar group, reduction in lipophilicity upon the incorporation of conventional ionic substituents, etc. remains a significant challenge. A study with a significant reduction in Φ has been reported upon the sulfonation of the chromophore[15a], and a reduction in the probe's sensitivity upon encapsulation is also evident. Overall, an ideal probe with balanced hydrophilicity-lipophilicity, easy preparation and high reproducibility is challenging and requires further research.

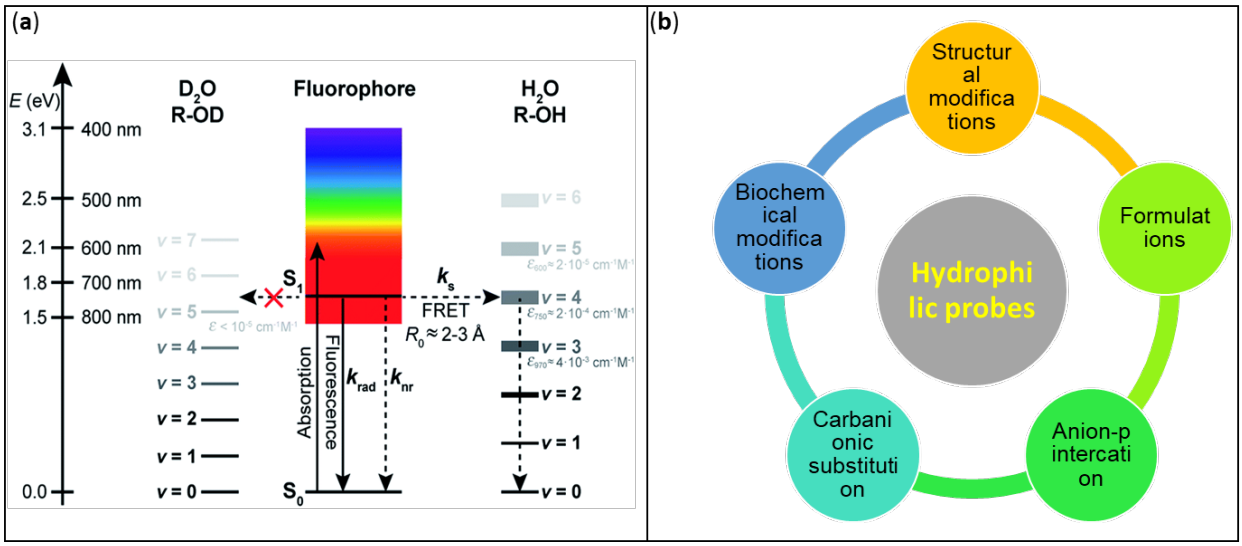

Figure 1: (a) Mechanism of solvent-assisted quenching in red-emitting fluorophores, (b) strategies to improve the water solubility of a probe. Reproduced from Ref. [16] with permission from the Royal Society of Chemistry.

3. Water soluble organic fluorophores with emission window in Vis-NIR-FIR region: Structural and photo-physical features

A probe with excellent photo-physical properties, high photostability, good balanced solubility profile, and biocompatibility is required prior to clinical applications. As mentioned earlier, OI fluorophores consist of extended π-conjugated systems responsible for absorption and emission over a wide range of wavelengths, i.e., visible (400–700 nm), first near-infrared (NIR-I, 700–1000 nm) and second near-infrared (NIR-II, 1000–1700 nm). Various water-soluble probes with emission in the visible region are available for academic and commercial purposes.[25] This includes but is not limited to Mito Tracker Green (MTG) ($\lambda_{abs.}/\lambda_{em}$ = 490/516 nm), Mito Tracker Red (MTR) ($\lambda_{abs.}/\lambda_{em}$ = 579/599 nm) and Mito Tracker Deep Red ($\lambda_{abs.}/\lambda_{em}$ = 644/665 nm. These probes also serve as a starting point for designing new emitters. Probes emitting in NIR-I and II windows attracted the interest of researchers and clinicians as they are better in terms of safety,

resolution, sensitivity, and interference with the biological matrices. NIR-based imaging probes are excellent candidates for fluorescence image-guided surgery and diagnostics. In literature, various reviews highlight the features, properties, and applications of organic, inorganic, and nanomaterial-based NIR probes.[26] We discussed recent examples of NIR I/II emitting dyes based on BODIPYs, Aza-BODIPYs, cyanine, CARBOPYs, and other heterocyclic cores. The sub-sections below discuss several examples of water-soluble dyes (with little or no organic solvent) with application in cancer diagnostics and therapeutics (theragnostic). The probes discussed herein are subdivided according to their backbone, as Dsouza, Pischel, and Nau used earlier.[27] Probes working via charge, electron, protons and energy transfer mechanisms and aggregation-induced emission (AIE) mechanism have been included.[27]

3.1. Coumarin and xanthene cores

Coumarin and xanthene have been extensively studied to prepare fluorescent dyes.[28] Although the parent coumarin core is non-fluorescent and hydrophobic, it can be judiciously functionalized to realize water-soluble emissive probes with an improved fluorescent quantum yield (Φ_F). While some probes are decorated with a targeting unit for selective delivery, some exploit the differences in cellular micro-environment, such as polarity, pH, viscosity, etc., to detect cellular abnormalities. It is a common knowledge that cancerous and normal cells have significant differences in behavior, properties, metabolism, and affinity towards endogenous and exogenous molecules. It has been noted that the cell's polarity is lost during tumorigenesis. [29] Based on this idea, Feng and colleagues [30] developed a polarity-sensitive probe **1** (Table 1) with a D-π-A structure. The probe can detect and respond according to the polarity of the cell membrane. The π-conjugated probe was composed of functionalized coumarin unit (hydrophobic polarity sensitive core), pyridine (an electron-withdrawing) and quaternary ammonium salt (hydrophilic) units. While there were no significant differences in the absorption profile in different media, the emission position was (strong fluorescence with relatively short wavelengths in low polar solvents and weak fluorescence with long emission wavelengths in highly polar solvents). It was noted that extending the hydrophobic core using tetrahydro quinoxaline and changing the lipophilic core produces polarity-sensitive probes **2a,b** (Table 1).[31] Including an electron-donating rigid tetrahydroquinoxaline group enhanced the ICT process, leading to a red shift of the emission wavelength. This is expected for a D-π-A type system. Absorption spectra of both compounds displayed a strong peak at $\lambda_{max.}^{Abs.}$ = 455 and 460 nm for **2a** and **2b**, respectively in water while it was slightly red shifted in THF (457-459 nm). It was noted that the emission intensity decreased

and bathochromically shifted with the solvent polarity ($\lambda_{max.}^{Emis.}$ = 605 nm for **2a** 607 for **2b,** Stoke shift $= 147\ \mathrm{nm}$) for **2a** and **2b,** in H_2O respectively).

Xanthenes are well known for their high singlet oxygen quantum yield and utility as triplet photosensitizers (PSs) in PDT.[9f] Some prominent examples of these dyes include fluorescein, eosin yellow, rose Bengal, erythrosin B and rhodamine.[32] Probe **3** (Table 1) is a dye that dissolves readily in water due to its zwitterionic structure. [33] In water, compound **3** showed a highly intense peak at $\lambda_{max.}^{Abs.}$ = 572 nm (ε = 3.81 × 10^4 M^{-1} cm^{-1}) and emission at $\lambda_{max.}^{Emis.}$ = 620 nm (ϕ = 0.18). The absorption peak position and intensity vary as a function of the pH of the solution (higher absorption at lower pH and *vice versa*). It was also demonstrated that compound **3** could be easily modified to prepare other structural analogues with metal ion and hydrazide sensing ability. It has also been shown that replacing the oxygen (O) atom at the 10 position with silicon (Si) in fluorescein derivative TokyoGreens produces a new generation of dye TokyoMagenta with absorption shifted by > 100 nm to the red.[34] Several Si-derived fluorescein derivatives have been reported and reviewed recently.[35] Recently, Cetin et al.[36] found that the iodination of the silicon-fluorescein core produces a bimodal probe **4** (Table 1) with fluorescence imaging capability and photocytotoxicity. Indeed, heavy atoms (iodine) cause intersystem crossing (ISC). Probe **4** existed in intramolecular spirolactone form at acidic pH values leading to negligible absorption/emission. However, at physiological pH (pH = 7.4), dianion (open-form) formed with an intense absorption ($\lambda_{max.}^{Abs.}$ = 614 nm, ε = 7.65 × 10^4 M^{-1} cm^{-1}) and emission ($\lambda_{max.}^{Emis.}$ = 630 nm, ϕ = 30%). Probe **5** (Table 1) is a highly sensitive rhodamine-based water soluble probe that shows turn on behavior in the presence of hypochlorite and was able to target mitochondria.[37] Absorption and emission spectra of **5** showed an enhancement in the peaks at 603 and 637 nm, respectively attributed to hypochlorite induced breaking of spirolactam structure to yield emissive species. The enhancement in the signal was proportional to the analyte concentration and the changes were fast with outstanding sensitivity (limit of detection 0.9 nM) and selectivity. Besides, some other works also demonstrated the analyte sensitive PL changes in xanthene-based probes.[38]

219 **Table 1**: Chemical structure, photophysical parameters, and applications of some water-soluble coumarin and xanthene-based fluorophores.

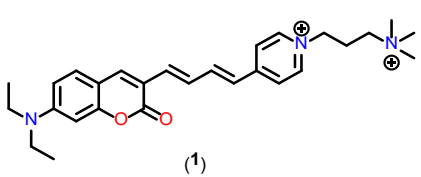
(**1**)

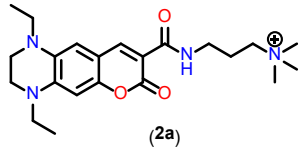
(**2a**)

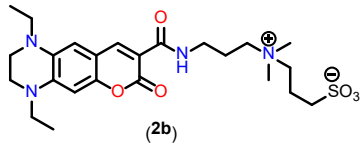
(**2b**)

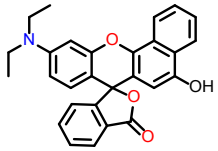
(**3**)

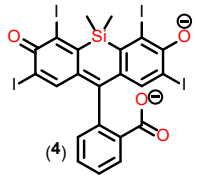
(**4**)

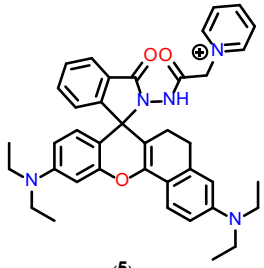
(**5**)

Comp. #	Photo-physical parameters				Application	Operating mechanism/Notes	Ref.
	$\lambda_{max.}^{Abs.}$, nm (solvent)	$\lambda_{max.}^{Emis.}$, nm (solvent)	Stokes shift (nm)	Fluorescence QY, Φ_F (solvent)			
(1)	506 (H_2O)	679 (H_2O)	173	0.008[a] (H_2O)	Monitoring cell membrane polarity; tumour imaging in animal models.	Polarity-dependent fluorescence change	[30]
(2a)	455 (H_2O)	605 (H_2O)	150	0.04[b] (H_2O)	Imaging cancer cell membranes and tumors.	Polarity-dependent fluorescence change	[31]
(2b)	460 (H_2O)	607 (H_2O)	147	0.04[b] (H_2O)			[31]
(3)	572 (H_2O)	620 (H_2O)	48	0.18[c] ($CHCl_3$)	Cell imaging.	pH-sensitive absorption change; Solvatochromic effect	[33]
(4)	614 (PBS + 0.5% DMSO)	630 (PBS + 0.5% DMSO)	16	0.11[d] (PBS + 0.5% DMSO)	Cell imaging; Photosensitization.	pH-dependent absorption and emission changes; Singlet oxygen generation	[37]
(5)	603 (PBS)	637 (PBS)	34	-	ROS (OCl^-) sensing in cellular and animal models.	ROS-dependent changes in absorption and emission profile	[37]

a: Rhodamine B in EtOH; b: Fluorescein in a 0.1 mM NaOH solution as the reference; c: In presence of 1% TFA; d: Methylene blue was used as a reference in PBS buffer as the reference

220

3.2. Boron–dipyrromethene (BODIPY) and related cores

Discovered around six decades ago, boron–dipyrromethene (BODIPYs) has been investigated for various technological applications owing to its bright fluorescence, narrow emission bandwidth, resistance to photobleaching, and environmental insensitivity. It is a well-known core in materials research as it is easy to functionalize and possesses intense and tunable absorption/emission profiles covering a broad spectrum.[39] Owing to their electron-deficient nature, they naturally tend to bind to organelles with negative potential, such as mitochondria. [40] A typical BODIPY core is hydrophobic but can be judiciously tuned to realize hydrophilic compounds. However, as stated earlier, tuning water solubility without affecting lipophilicity and photophysical properties is daunting. Some common strategies to enhance the aqueous solubility while maintaining the PL properties include the introduction of steric hindrance, electrostatic repulsions and Boron functionalization. For example, Ulrich and coworkers [41] reported a series of pH-responsive BODIPYs with styryl substituents at proximity and positively charged tertiary amine groups at the B-centre. Such arrangement led to steric hindrance and electrostatic repulsion, thus preventing the formation of dark aggregates. Indeed, the presence of sulfobetaine at B-center enhanced the water solubility of the compounds. In H_2O, compounds absorbed between 567-697 nm while emitted between 582-826 nm. Despite these favourable features, no application was tested. Wang et al.[40] demonstrated that the water solubility of a probe is an essential factor for targeting mitochondria and should be considered while designing the probes. For example, **6** (Table 2) is a π-expanded water-soluble dye that shows intense bands in the visible region, with $\lambda_{max.}^{Abs.}$ = 617 nm and an emission at $\lambda_{max.}^{Emis.}$ = 630 nm (τ = 4.3 ns, Φ = 43%). The solubility and blue shifted absorption were attributed to the quaternary amine group that caused the ICT-effect. Considering the solvent, these data prove that **6** is better than native BODIPY and commercially available dye Mito Tracker Red dye ($\lambda_{abs.}$/ λ_{em} = 579/599 nm in DMSO). Besides, **6** was a more biocompatible, chemically and photostable candidate than commercial dyes. It was found that the solubility and targetability can also be modulated using only TPP groups.[42] For example, probe **7** (Table 2) is the first example of a multiple bulky cationic group (TPP) containing water-soluble probes with $\lambda_{abs.}$/ λ_{em} = 651/673 nm. As expected for the probes in the aqueous system, it showed weak fluorescence (Φ = 1.7%) in water but high in organic media, with Φ_F higher for probes with greater TPP units. Moreover, TPP moieties also enhanced the membrane permeability, chemically and photostability. Bardon et al.[23] reported π-extended (at position 3) dye **8** (Table 2) containing water-solubilizing charged groups (at position 8). Like the previous example, they also noted that the properties of dicationic-containing dye were better than the neutral counterpart. Probe **8** showed different absorption and emission features in water and surfactants. For instance, it

emitted very weak in water; a strong emission (like organic solvents) was noted in 0.7% Triton X-100 (but not in SDS).

Table 2: Chemical structure, photophysical parameters, and applications of some water-soluble BODIPY-based fluorophores.

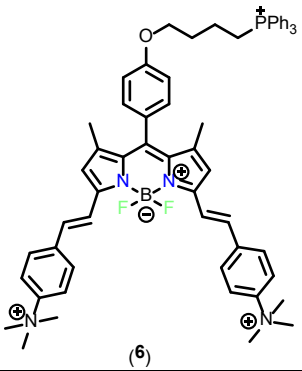

(**6**)

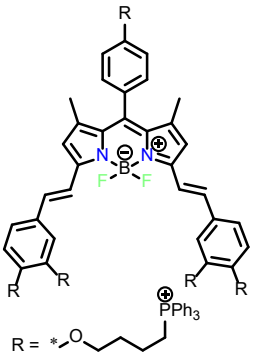

(**7**)

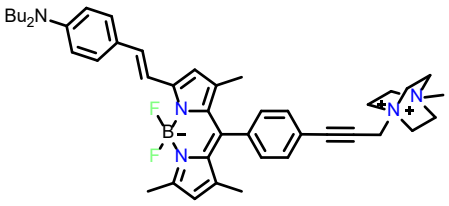

(**8**)

Comp. #	Photo-physical parameters				Application	Operating mechanism/Notes	Ref.
	$\lambda_{max.}^{Abs.}$, nm (solvent)	$\lambda_{max.}^{Emis.}$, nm (solvent)	Stokes shift (nm)	Fluorescence QY, Φ_F (Lifetime)			
(6)	617 (H_2O)	630 (H_2O)	13	0.43 (4.3 ns)	Monitoring cell membrane polarity; tumour imaging in animal models.	Polarity-dependent fluorescence change, ICT effect. -	[40]
(7)	651 (H_2O)	673 (H_2O)	22	1.7[a]	Mitochondrial imaging, Protein (BSA) labelling,	Fluorescence "*turn-on*".	[42]
(8)	630 ($CHCl_3$)	690 ($CHCl_3$)	(-)	0.55	Plasma membrane labelling.	Non-emissive in water but highly fluorescent upon insertion to extracellular leaflet.	[23]

a: Oxazine 170 was used as the reference in methanol.

Aza-BODIPYs are a new generation of BODIPY derivatives in which meso carbon at position 8 is replaced by N-atom with a superior PL profile. However, like other organic imaging probes, they hold low water solubility, necessitating surfactant use. To solve the problem, Goze and coworkers [22] reported a new class of Aza-BODIPYs probes, known as Wazaby, bearing phenyl (at 1 and 3) and methoxyphenyl (at 3 and 5) positions. Like earlier examples of BODIPYs, they noted that the judicious engineering at B-center yielded water soluble and stable **9a,b** (Table 3) with photophysical properties better or comparable to Aza-BODIPys. In PBS, **9a** showed absorption

peaking at 676 nm and emission at 712 nm (Φ = 0.09) while **9b** at 673 nm and 714, respectively. Bioconjugated probes containing diethyl squarate as the conjugating handle were also reported using these two probes, which exhibited similar emissions. Motivated by the results, the same group reported **10** (Table 3) with properties and features better than one with BF_2 core, indicating the advantages of B-functionalization.[24] Interestingly, this probe showed a better emission profile in plasma than PBS with absorption and emission maxima at 746/867 nm and extended to 1200 nm (Φ = 2.5%, (Fig. 2a), attributed to the torsional restriction of the probe. The same group reported human epidermal growth factor receptor 2 (HER2) targeting dye **11** (Table 3) by conjugating trastuzumab antibody. [43] Compared to **10**, this was brighter and showed red-shifted emission (802/846 nm in PBS with 10% serum).

Table 3: Chemical structure, photophysical parameters, and applications of some WAZABY fluorophores.

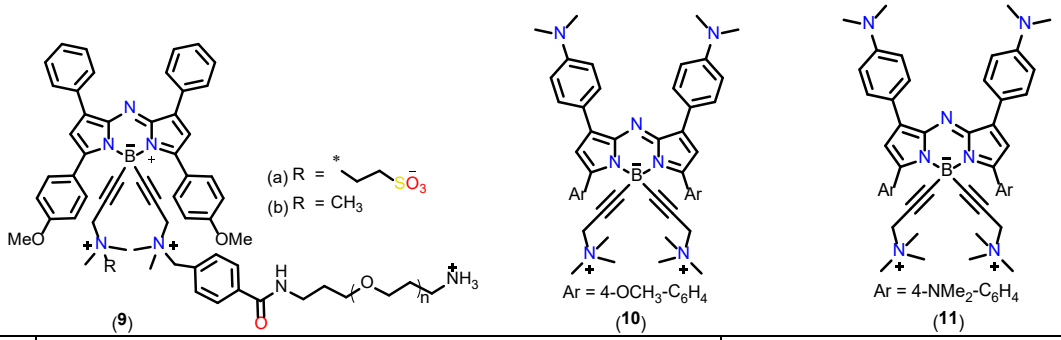

(**9**) (**10**) (**11**)

Comp. #	Photo-physical parameters				Application/Notes	Ref.
	$\lambda_{max.}^{Abs.}$, nm (solvent)	$\lambda_{max.}^{Emis.}$, nm (solvent)	Stokes shift (nm)	Fluorescence QY, Φ_F (Lifetime)		
(9)	676, 673 (PBS)	712, 714 (PBS)	36-41	0.09, 0.07 (PBS)	Bioconjugated to antibodies to image PD-L1 (Programmed Death-Ligand 1)	[22]
(10)	746 (PBS + 10% plasma)	867 (PBS + 10% plasma)	121	0.025 (PBS + 10% plasma)	In vitro and in vivo imaging, NIR-II fluorescence imaging	[43]
(11)	802 (PBS + 10% plasma)	846 (PBS + 10% plasma)	44	(-)	Tumor imaging, fluorescence-guided surgery (FGS), targeting human epidermal growth factor receptor 2 (HER2)-positive ovarian tumors	[43]

Recently, Guo and workers [44] found that the replacement of B → C in lipophilic BODIPYs generates a new generation of cationic dyes **12-14** (Table 4), known as CARDIPYs, with improved solubility, high brightness and tunable photophysical properties. Compound **12a-c** ($\lambda_{abs}/\lambda_{em}$ = 493-494/510 nm, Φ = 0.84-0.98 in PBS), mono styryl-derivative **13a-c** ($\lambda_{abs}/\lambda_{em}$ = 561-584/577-633

nm, Φ = 0.05-0.96 in PBS) and distyryl-substituted **14a-c** ($\lambda_{abs}/\lambda_{em}$ = 636-673/654-713 nm, Φ = 0.19-0.57 in 80% PBS) showed an expected red-shifted absorption and emission (due to π-extension) and did not show any aggregation in PBS like the B-counterparts (Fig. 2b-d). These dyes showed high ε and brightness too. Their cationic character imparted higher solubility and high stability against photo-bleaching.

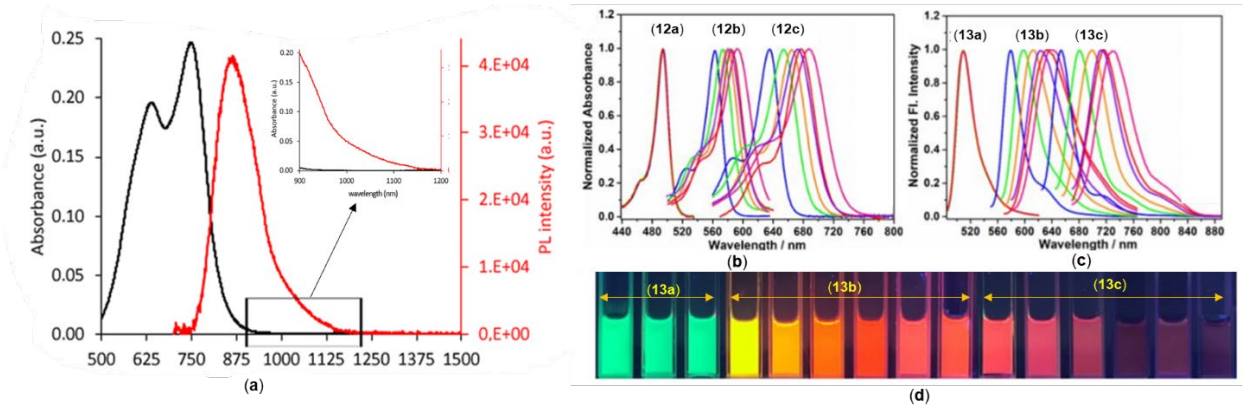

Figure 2: (a) Absorption spectra and emission spectra of (a) **10** and (b, c) CARDIPYs **12a-c** and **13a-c**. (d) Fluorescence colors of probes **13a-c** under UV lamp. For further details, see original references. Reprinted with permission from Godard A, Kalot G, Pliquett J, Busser B, Le Guevel X, Wegner KD, Resch-Genger U, Rousselin Y, Coll JL, Denat F, Bodio E, Goze C, Sancey L., *Bioconj. Chem*. 2020, 31, 4, 1088–1092. Copyright 2020 American Chemical Society and Zhang H, Liu J, Sun Y-Q, Liu M, Guo W. *J. Am. Chem. Soc*., 2020, 142, 40, 17069–17078. Copyright 2020 American Chemical Society.

Table 4: Chemical structure, photophysical parameters, and applications of CARDIPYs.

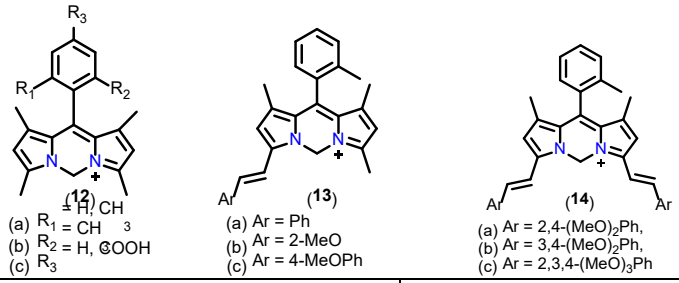

Comp. #	Photo-physical parameters				Application/Notes	Ref.
	$\lambda_{max.}^{Abs.}$, nm (solvent)	$\lambda_{max.}^{Emis.}$, nm (solvent)	Stokes shift (nm)	Fluorescence QY, Φ_F (Lifetime)		
(12)	493-494 (PBS)	509-510 (PBS)	16	0.84-0.91[a] (4.59-7.53)	In vitro imaging of mitochondria	[44]
(13)	561-584 (PBS)	577-633 (PBS)	16-49	0.05-0.96[b] (2.28-7.28)	In vitro imaging of mitochondria to the lysosome	[44]
(14)	636-670 (80% PBS)	654 - 710 (80% PBS)	18-41	0.19-0.57[c] (3.00-5.51)	In vitro imaging of mitochondria-to lysosome and mitochondria only.	[44]
a: Fluorescein; b = cresyl violet; c = Cy5.5 as the reference						

3.3. Cyanine and related cores

Cyanines are indoline-based dyes that covers the visible-NIR spectral region, have low toxicity, and excellent applications in imaging.[45] For example, indocyanine green (ICG) is a heptamethine cyanine dye used to visualise breast cancer and melanoma.[45] However, like other π-conjugated systems, these dyes aggregates in an aqueous environment show low Φ, short retention time, and complicated and multi-step derivatization. Various modifications and cyanine-containing cores have been reported to overcome these challenges. Probe **15** (Table 5) is a semi-cyanine based water-soluble probe that can detect proteolytic L-aminopeptidases (LAP) without any aid modern instrument (i.e., naked eye detection) under physiological conditions.[46] The probe design included an emission unit attached to L-leucine (recognition fragment) through a self-immolative and LAP-sensitive group (*p*-amino benzyl alcohol). Free **15** shows an absorption band at 405 nm (light red), which, in the presence of LAP, diminished this peak, and a new band at 535 nm appeared, and the colour of the system changed to pink-red. A similar kind of observation was noted in the emission profile. Upon excitation at 530 nm, weak fluorescence (Φ = 0.010) at 607 nm was observed. After exposure to LAP (0.15 UmL^{-1}), a significant fluorescence enhancement at 625 nm was noted (Fig. 3a,b). Overall good stability under these physiological conditions, low detection limit (50 ng/mL), high selectivity, and safe nature were the main features of the probe. Wang and coworkers [47] prepared a water-soluble dye **16** (Table 5) composed of dipeptide (Cys-Leu: Cysteine-Leucine) attached to a semi-cyanine core. This dye showed excellent sensitivity (enhancement in emission intensity) towards LAP. Photophysical studies in PBS at physiological pH and 37 °C showed an intense absorption peak in the visible region (578 nm) with a weak emission at 701 nm. However, a dramatic increase in emission and a decrease in absorption peak (578 nm) were noted within a short time (9 mins) upon the addition of LAP. It was suggested that LAP cleaved the amide bond and formed an emissive phenolic semi-cyanine core. Licha and coworkers [48] introduced a redox-sensitive group into the meso-position of an indodicarbocyanine dye to realize "*on-off-on*" probes **17** and **18** (Table 5). Mechanistically, it utilized the redox-sensitive properties of hydroquinone (**17**) and catechol (**18**), which oxidized to *o*- or *p*-quinone, leading to a change in the emission (Fig. 3c). These two water-soluble sulfonated dyes display absorption and emission maxima at 640/644 nm and 661/669 nm, respectively.[48] Another "*off–on*" probe **19** (Table 5 and based on 7-nitro-1,2,3-benzoxadiazole (NBD) that shows a response against endogenous H_2S (not biothiols) with high specificity against prostate-specific membrane antigen (PSMA) have been recently reported (Fig. 3e-f).[49] With high solubility in PBS (up to 40 μM) and absorbance in the visible region (520 nm and 700 nm), this probe displays weak emission (Φ = 0.001) in PBS due to the quenching by NBD core. However, upon the

interaction with H_2S, a new peak at 535 nm was noted with a red-shifted low energy absorption peak and enhancement in the emission at 803 nm (Φ = 0.047). The attachment of the PSMA unit as the targeted unit did not alter the photo-physical properties but enhanced the probe's selectivity.[50]

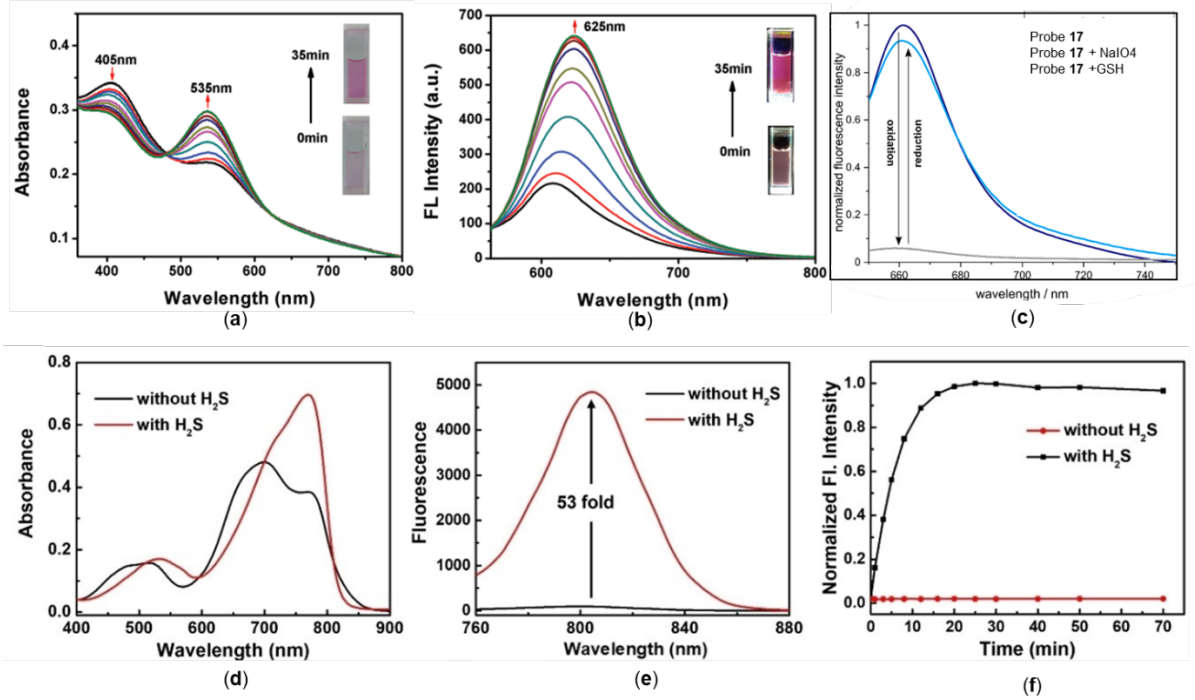

Figure 3: Changes in the absorption of (a) probe **15** in the presence of LAP enzyme in aqueous solution. Emission changes in (b) probe **15** and (c) probe **17** upon adding LAP enzyme and $NaIO_4$/GSH, respectively. (d,e) Absorption and emission spectra of **19** (10 μM) in PBS, (f) Changes in emission intensity of **19** at 803 nm in the presence and absence of H_2S. For further details, see original references. Reproduced with permission from ref. [46, 48-49]

Table 5: Chemical structure, photophysical parameters, and applications of hemicyanine and cyanine dyes.

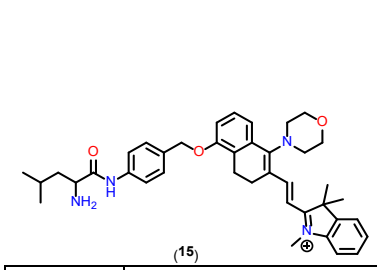
(15)

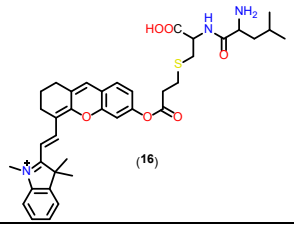
(16)

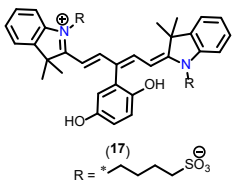
(17)

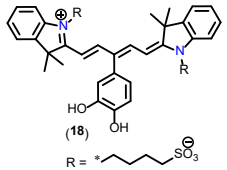
(18)

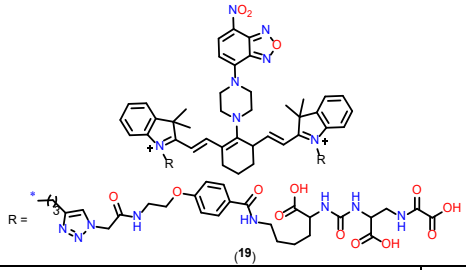
(19)

Comp. #	Photo-physical parameters				Application	Operating mechanism/Notes	Ref.
	$\lambda_{max.}^{Abs.}$, nm (Medium)	$\lambda_{max.}^{Emis.}$, nm (Medium)	Stokes shift (nm)	Fluorescence QY, Φ_F (solvent)			
(15)	405, 535 (PBS)	607 (PBS)	42	0.01	Cell imaging; monitoring of enzyme.	Absorption and emission changes	[46]
(16)	578 (PBS)	701 (PBS)	123	(-)	In vitro imaging, monitoring Enzyme activity	Absorption and emission changes	[47]
(17)	640 (PBS)	661 (PBS)	21	0.08	Biologically relevant reducing species, reduction-sensitive probe for bioimaging in living cells	pH and reduction-sensitive fluorescence switching	[48]
(18)	644 (PBS)	669 (PBS)	25	0.06			
(19)	520, 700 (PBS)	803 (PBS)	103	0.001[a]	H_2S activity in cells, animal model	H_2S-mediated absorption and emission changes	.[49]
a = ICG as the reference.							

Probes emitting in the second near-infrared window (NIR-II, 1000–1700 nm) are considered much better than visible/NIR-I counterparts as they offer diminished auto-fluorescence, suppressed photo-scattering, improved resolution, deeper penetration with ultra-low background interference. However, realizing such fluorophores with solubility and stability in biological media is quite challenging. This is why most of the NIR-II probes are formulated (e.g. nano-formulation) prior to imaging studies. Probe **20a** (Fig. 4a) is a heptamethine cyanine-based sulfonated zwitterion probe. However, it has low stability due to the chemically labile O-aryl linker, as it is susceptible to cleavage by biological nucleophiles. To solve this riddle, Smith and coworkers [51] employed the idea of molecular strapping to protect dye form degradation and use in animal settings. Dye **20b** ($\lambda_{abs.}/\lambda_{em}$ = 769/788 nm, Φ = 11.0%, MB = 23000 in PBS, Fig. 4b) showed better performance than **20a** ($\lambda_{abs.}/\lambda_{em}$ = 768/785 nm, Φ = 9.0%, MB = 18000 in PBS). The other unique feature was the intramolecular lattice packing distance in solid state. It was noted that the distance between the adjacent fluorochromes in **20b** was almost double than the normal heptamethine cyanine dyes, leading to the isolation of the fluorochromes. Similarly, dye **21a** (Fig. 4c) forms H-aggregates under physiological conditions and lacks a suitable protein conjugation site. To circumvent this problem, doubly strapped dye **21b** (Fig. 4d) was prepared with absorption/emission maxima >1000 nm ($\lambda_{abs.}/\lambda_{em}$ = 980/1015 nm, Φ = 0.014%, MB = 19 in PBS), outperforming the unstrapped counterpart **21a** ($\lambda_{abs.}/\lambda_{em}$ = 1046 and 810 /1080 nm, Φ = 0.0594% in FBS).[52] Moreover, these dyes with double straps can be conjugated to proteins without causing unwanted degradation or change.

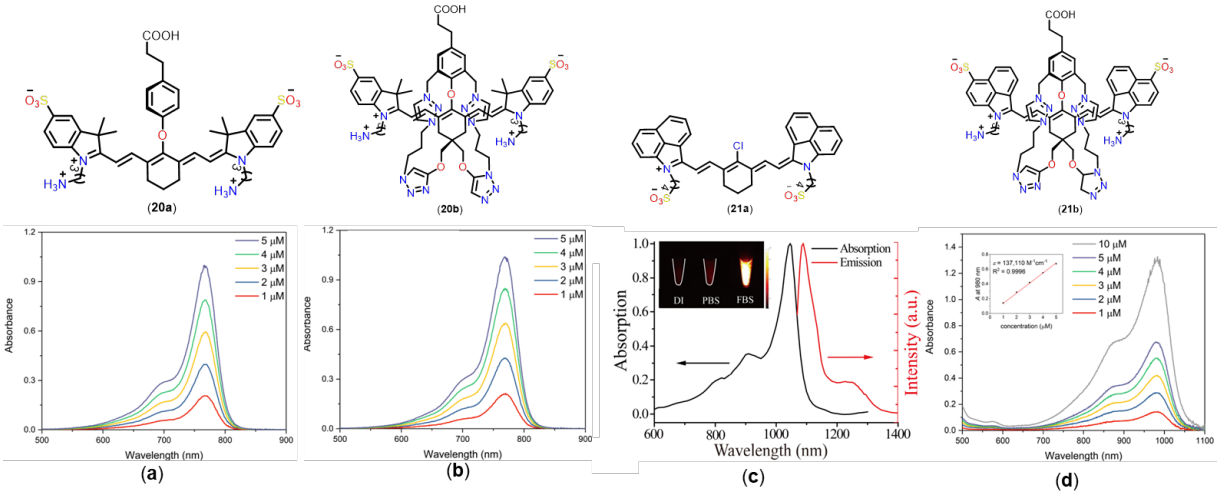

Figure 4: Chemical structures of 20a,b and 21a,b. Absorption spectra of unstrapped (a) 20a, (c) 21a and strapped 20b (b) and 21b (d) dyes. Reproduced with permission from ref. [51-52]

While most modified dyes in the literature have centrally modified meso cores, researchers have also investigated dyes with changes in the lateral indoline units. For example, it was noted that using a strong donor (indolizine) significantly affects the photo-physical properties and shows red-shifted absorption/emission, higher brightness, and photo-stability. Examples include probes **22** and **23** (Fig. 5a and 5b). [53] As compared ICG ($\lambda_{abs.}$/ λ_{em} = 798/897 nm, Φ = 9.3% in FBS) **22** ($\lambda_{abs.}$/ λ_{em} = 842/808 nm, Φ = 0.1% in FBS) and **23** ($\lambda_{abs.}$/ λ_{em} = 719/720 nm, Φ = 58.3% in FBS) displayed better properties. On the other hand, **23** (MB = 65900) displayed excellent brightness in FBS too. Combining the strategy of a changeable π-conjugated system and introducing benzoic moiety, Ma and co-workers [54] reported water-soluble conjugated polymethine probes **24a-c** and **25** (Fig. 5c and d) by condensing two rhodamine fragments. Compared to others, **24a** ($\lambda_{max.}^{Abs.}$ = 585, 740 nm) display inferior PL properties, solubility and stability, attributed to the absence of hydrophilic *ortho*-PhCOOH. Even though compound **24** displayed bathochrmically shifted absorption ($\lambda_{max.}^{Abs.}$ = 700, 850 nm) owing to extended π-conjugation, it exhibits nearly flat emission in the PBS, thereby limiting its biological applications. **24b** ($\lambda_{max.}^{Abs.}$ = 595, 740 nm $\lambda_{max.}^{Emis.}$ = 940 nm, MB = 3.8, Φ = 0.0002) and **24c** ($\lambda_{max.}^{Abs.}$ = 660, 760 nm and $\lambda_{max.}^{Emis.}$ = 1040 nm, MB = 1.5, Φ = 0.00004) showed performance in terms of brightness, fluorescence, aqueous solubility and stability. The designed probe was useful for NIR vasculature imaging, dynamic imaging of blood circulation and organs, and LAP enzyme imaging.

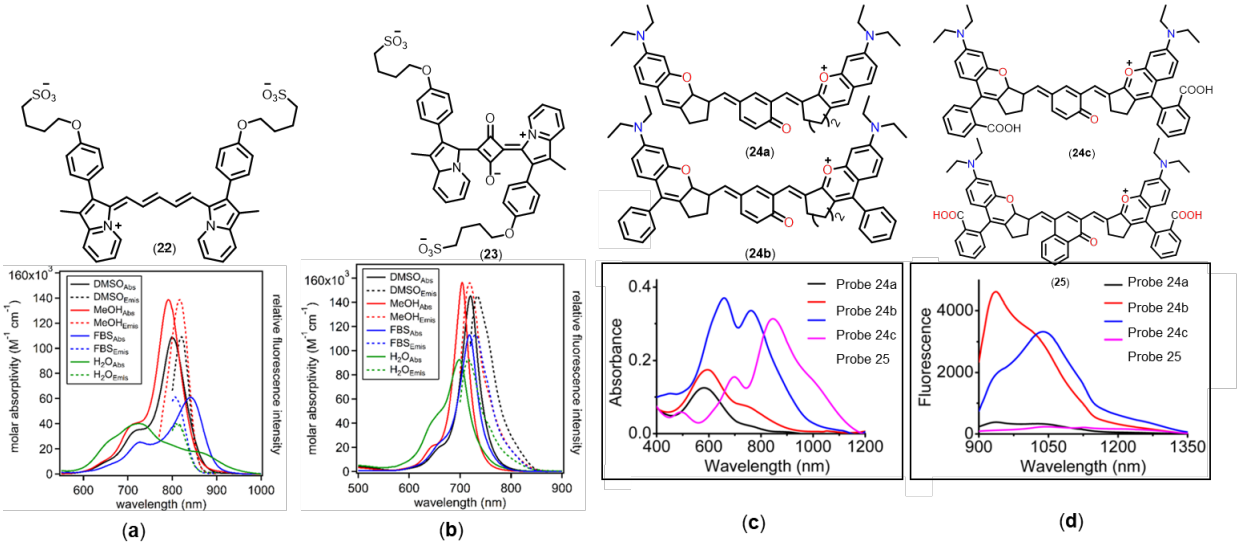

Figure 5: Chemical structure, absorption, and emission profiles of 22-25. Reprinted with permission from Meador WE, Autry SA, Bessetti RN, Gayton JN, Flynt AS, Hammer NI, Delcamp JH. J. *Org. Chem*. 2020, 85, 6, 4089–4095. Copyright 2020 American Chemical Society. Reproduced with permission from ref.[54]

3.4. Benzothiadiazole (BTD) cores

Among many heterocyclic cores, 2,1,3-benzothiadiazole (BTD) has been a subject of interest in research by materials and medicinal chemists. Lower band-gap ($E_g^{op.}$), tunable rigid structure, electron accepting nature etc. makes this candidate an ideal choice for the development of fluorophores.[55] Neto and co-workers[56] reported a series of BTD-based neutral **26** (Table 6) and charged **27a-c** (Table 6) probes with $\lambda_{max.}^{Abs.}$ = 362-367 nm and emission at $\lambda_{max.}^{Emis.}$ = 538-552 nm (Stokes shift = 171-190 nm) in water. Theoretical study revealed that the LUMO was based on acceptor centered on the BTD core while HOMO was distributed not beyond **26**, indicating no effect of the alkyl chain length on the low energy π-π* transition. The attachment of a lipophilic anchor (TEG) to pyridine N along with a hydrophilic anion ($MeSO_3^-$) produced a water-soluble dye **27d** (Table 6) with ICT characteristics.[57] This probe showed a slightly red-shifted absorption ($\lambda_{max.}^{Abs.}$ = 370 nm) with an green emission maxima at $\lambda_{max.}^{Emis.}$ = 543 nm (Φ = 0.01) and stokes shift = 173 nm in water. Probe **27d** was found to be an effective water-soluble and selective bioprobe for plasma membrane imaging. Following this work, the same group [58] found that imidazolium-based ionic liquids-containing BTD **28a-c** (Table 6) shows excellent subcellular localization. The introduction of imidazolium cations was found to fine-tune the chemical, physical properties, thermo- and photo- stabilities, hydrophobicity-hydrophilicity, and molecular geometries. They showed absorption between 333-362 nm in water with emission maxima at 430-453 nm. A hybrid **29** (Table 6) [59] containing γ-Glu group (GGT recognition unit) and indocyanine-BTD fluorophore was turned on upon the presence of cell-surface enzyme GGT. Probe **29** showed good water solubility and displayed a strong absorption band (438 nm) which undergoes a red shift (73 nm) and hypochrmosim upon the addition of GGT.

Using two different type of acceptors (6,7-bis(4-(hexyloxy)phenyl)-4,9-di-(thiophen-2-yl)-[1,2,5]thiadiazolo[3,4-g]quinoxaline and thienoisoindigo) and four different donors (thiophene, triphenylamine, 9,9-dioctyl-9H-fluorene, or 2-(9,9-dioctyl-9H-fluoren-2-yl)thiophene), Sun and coworkers[60] reported a series of D-A-D type of probes **30a-d** (Table 6) with excellent photo-physical properties and PEG-modified to achieve water solubility. The optical properties of the PEGylatd counterpart were similar in both organic and aqueous phase. As demonstrated in the earlier examples, one-atom replacement is an intriguing strategy to realize in cores with improved PL properties. Liu *et al*. [61] replaced the oxygen atom of an established donor 3,4-ethylenedioxy thiophene (EDOT) with sulphur to realize 3,4-ethylenedithio thiophene (EDST) and constructed D–A–D type fluorophore, **31** (Table 6). Interestingly, this O→S modification led to an increase in Φ. Despite ethe fact that small organic fluorophores were insoluble in water, the encapsulated

nano-probe displayed superb NIR-II features ($\lambda_{abs.}$/ λ_{em} = 768/1053 nm, Φ = 0.27% for **31a** and 724/1043 nm, Φ = 1.3% for **31b** in water). The replacement of oxygen by S affects optical features, and replacing the ethylenedioxy group with simple alkyl modulates the absorption and emission values. Xia and coworkers [62] reported nano-probes **32a-c** (Table 6)[62] with high brightness and NIR-II imaging ability. The probe showed AIE effect in solution due to using TPA as laterally shielded groups. **32c**-based nanodots showed emission with a tail extended to 1600 nm in water, detectable at multiple wavelengths (1320 nm and 1550 nm wavelength LP filters). Hong and coworkers[63] reported the preparation and application of PEGylated **33a** (Table 6), and RGD labelled targeted **33b** (Table 6) NIR-II probes. [63] They found that inserting 2-amino 9,9-disubstituted fluorene donors into the backbone remarkably enhanced the emission properties. **33a** showed λ_{em} = 1100 nm while **33b** (Table 6) at λ_{em} = 1050 nm. Structurally similar dye **34** (Table 6) having different central acceptor units has also been reported with $\lambda_{abs.}$ ~ 700 nm extended to 1000 nm.[64] Similarly, under the excitation of 808 nm, it showed emission maxima at λ_{em} = 1100 nm with a tail extended over 1300 nm (Φ = 0.06%). Another advantage of this probe included good biocompatibility and renal clearance.

Table 6: Chemical structure, photophysical parameters, and applications of water-soluble BTD-based fluorophores.

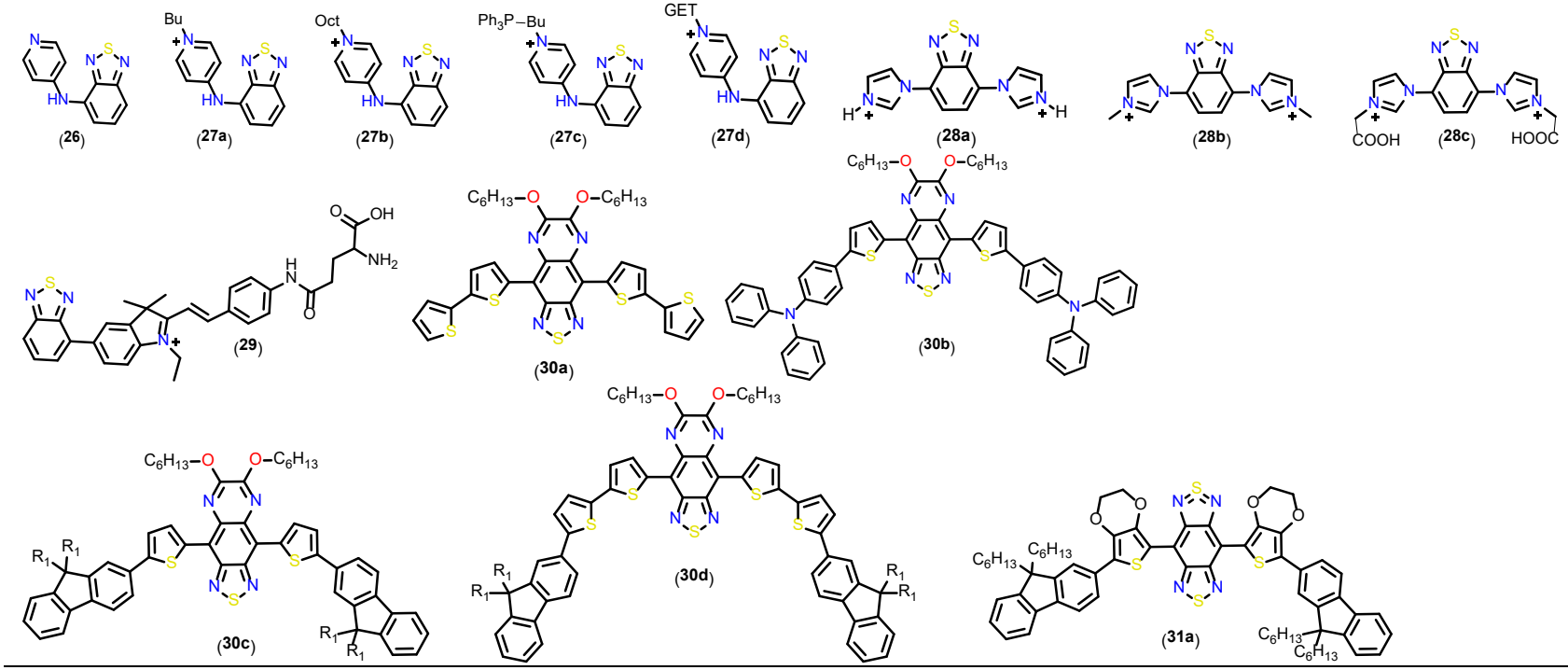

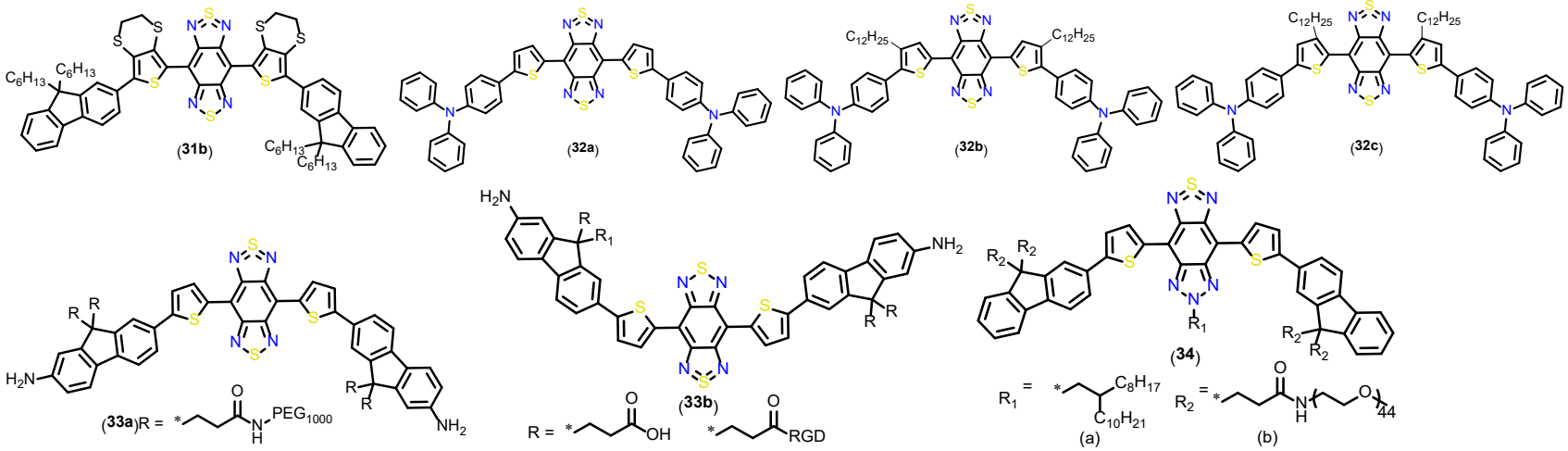

Comp. #	Photo-physical parameters				Application	Ref.
	$\lambda_{max.}^{Abs.}$, nm (solvent)	$\lambda_{max.}^{Emis.}$, nm (solvent)	Stokes shift (nm)	Fluorescence QY, Φ_F (solvent)		
(26)	362 (H_2O)	552 (H_2O)	190	0.001 (H_2O)	Cell imaging	[56]
(27a)	365 (H_2O)	550 (H_2O)	185	0.007 (H_2O)	Cell imaging	[56]
(27b)	366 (H_2O)	552 (H_2O)	186	0.005 (H_2O)		
(27c)	367 (H_2O)	538 (H_2O)	171	0.050 (H_2O)		
(27d)	370 (H_2O)	543 (H_2O)	173	0.01 (H_2O)		
(28a)	348 (H_2O)	453 (H_2O)	105	0.01 (ACN)[a]	Cell imaging	[58]
(28b)	333 (H_2O)	453 (H_2O)	120	0.01 (ACN)[a]		
(28c)	333 (H_2O)	450 (H_2O)	117	0.001 (ACN)[a]		
(29)	438, 512 (PBS)	578 (PBS)	(-)	(-)	GGT activity in living cells, absorption and emission changes	[59]

(30a)	644 (THF)	976 (THF)	332	0.0397 [b]	NIR imaging, latent fingerprint (LFP) imaging Vasculature, lymph node, vascular haemorrhage, and gastrointestinal tract.	[60]
(30b)	687 (THF)	1036 (THF)	349	0.03 [b]		
(30c)	655 (THF)	983 (THF)	328	0.0697 [b]		
(30d)	695 (THF)	997 (THF)	302	0.037 [b]		
(31a)	768 (H2O)*	1053*	285	0.0027 [c]	In vitro and in vivo imaging.	[61]
(31b)	724 (H2O)*	1043*	319	0.013 [c]		
(32a)	(-)	(-)	(-)	(-)	in vivo NIR-IIa and NIR-IIb imaging.	[62]
(32b)	(-)	(-)	(-)	(-)		
(32c)	734#	1002#	(-)	(-)		
(33a)	860	~1100	(-)	(-)	αVβ3-targeted glioma imaging, detecting sentinel lymph nodes.	[63]
(33b)	843	~1050	(-)			
(34)	707 (H_2O)	1000 (H2O)	293	0.0006 [b]	In vitro and in vivo NIR imaging.	[64]
a: Quinine sulfate as the standard in H_2SO_4; b = IR1061; c = relative to IR26						

454

3.5. Other aromatic and heteroaromatic cores

Numerous carbon-rich probes with excellent photophysical features but with limited/no water solubility are reported in the literature. One of them is tetraphenylethene (TPE), which is well-known for aggregation-induced emission (AIE)/aggregation-enhanced emission (AEE). Tang and coworkers [65] reported *N*-oxide-bearing TPE probes that show hypoxia-responsiveness. The fact that N-oxides undergo two-electron reduction and form emissive solids was utilized to image oxygen levels in the HeLa cells. Tan et al.[66] reported AIEgens based on TPE-based probe **35** (Table 7) that could be used to detect reactive oxygen species (ROS), especially hypochlorite (ClO^-). In the aqueous system, owing to AIE, it showed high emission, which diminished upon the interaction with ClO^-, attributed to the conversion of thiourea to urea. In PBS, probe **35** exhibits intense emission (maxima ~ 492 nm) which reduced to half in DCM and hexane with blue shifted maxima (400-420 nm). Perylene-3,4,9,10-tetracarboxylic diimide **36** (Table 7) is a fluorescent probe for determining pH changes. [67] In water, this probe showed a different absorption profile (($\lambda_{max.}^{Abs.}$ = ~ 500 nm and 535 nm and a broad shoulder at 473 nm) than in organic solvent (460, 490 and 520 nm), indicating nano-aggregate formation. However, the absorption profile was insensitive to pH, and the emission profile varied significantly due to PET. The emission intensity was high at a lower pH (Φ = 0.003) but diminished at a higher pH (Φ = 0.11). Despite its low toxicity, it was found that the PDI probe is cell permeable (L929 cells) only at lower concentrations and did not induce intracellular fluorescence lightning at higher PDI concentrations. Combining the hydrophilic amino pharmacophore of mitoxantrone and the aminonaphthalimide scaffold of amonafide, Johnson et al.[68] reported napthalimide-based probes **37-39** (Table 7). The developed probe showed excellent photo-physical properties in polar and non-polar solvents. For instance, in water, they showed pH-sensitive broad absorption ($\lambda_{max.}^{Abs.}$ = ~ 398-448 nm at pH 11 and 387-434 at pH 4 and emission profile ($\lambda_{max.}^{Emis.}$ = 538-540 nm, ϕ = 47-58%) large Stoke shifts (98-145 nm) with blue (in hexane) to orange (in water) color emission. The compounds function as fluorescent pH probes based on PET and/or ICT.

Due to its highly conjugated structure, lower LUMO level, red-shifted absorption, and high thermal stability, silicon-bridge fluorene analogue is a common motif in opto-electronic research.[69] Considering these unique features, Auvray et al.[70] studied the properties and applications of quadrupolar (A-π-D-π-A) silafluorene dyes **40a,b** (Table 7). The reported probes were highly water soluble and showed no aggregation up to 180 μM. Photophysical studies revealed that the **40b** exhibited red-shifted optical characteristics ($\lambda_{max.}^{Abs.}$ = 416 nm, $\lambda_{max.}^{Emis.}$ = 535 nm, ϕ = 13%) than **40a** ($\lambda_{max.}^{Abs.}$ = 345 nm, $\lambda_{max.}^{Emis.}$ = 530 nm, ϕ = 3%) in water. Also, the former dye

exhibited almost ~4.6 times more brightness than the later. Besides, probe **40b** (2100 GM at 740 nm) exhibits a much larger large two-photon (2PA) cross-section than **40a** (not detectable).

Thiophenes, bithiophenes, terthiophenes and thienothiophenes are electron-rich materials with excellent photophysical properties. Many D-π-A and D-A molecules with unique luminescence properties and applications are available in the literature. It has been noted that sulfur oxidation moves its absorption and emission to the red. Motivated by this, Żurawiński and coworkers[71] investigated dithienothiophene *S*,*S*-dioxide **41** (Table 7) with a length close to the thickness of the phospholipid membrane for their suitability in fluorescent cell imaging. Compounds **41a** and **41b** were water soluble owing to the presence of polar/charged groups, absorption in the visible region (520 nm for both), and limited emission profile in water. Despite this, the compounds showed excellent cellular imaging ability without any modification in the standard cell culture. The same group reported compound **41c** with photo-physical properties similar to previous compounds but beneficial for imaging membranes. [72] Using two different type of acceptors (6,7-bis(4-(hexyloxy)phenyl)-4,9-di-(thiophen-2-yl)-[1,2,5]thiadiazolo[3,4-g]quinoxaline and thienoisoindigo) and four different donors (thiophene, triphenylamine, 9,9-dioctyl-9H-fluorene, or 2-(9,9-dioctyl-9H-fluoren-2-yl)thiophene), Sun and coworkers[60] reported a series of D-A-D type of probes **42a-d** (Table 7).

508 **Table 7**: Chemical structure, photophysical parameters, and applications of some water-soluble aromatic and heteroaromatic
509 fluorophores.

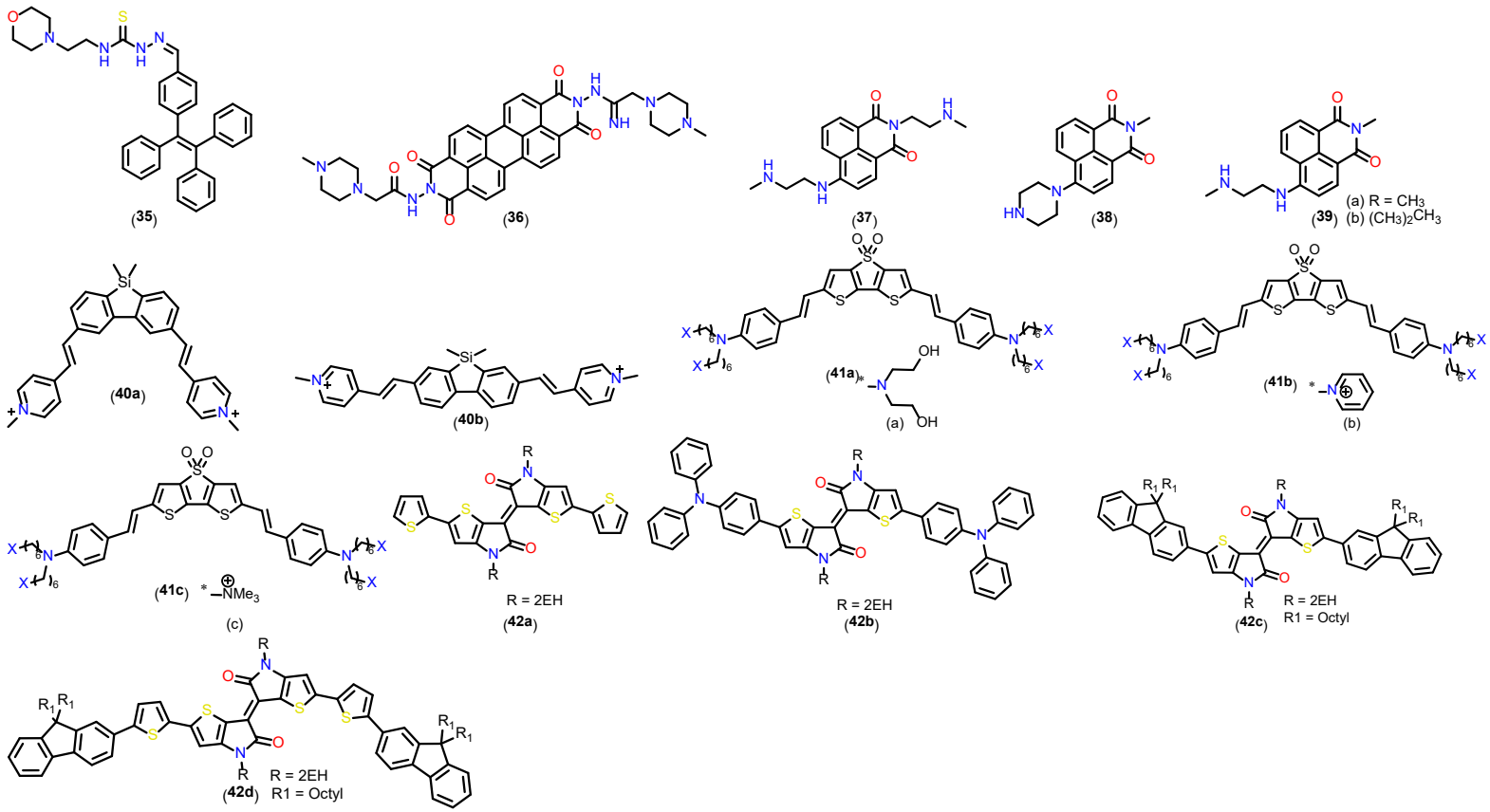

Comp. #	Photo-physical parameters				Application/Notes	Ref.
	$\lambda_{max.}^{Abs.}$, nm (solvent)	$\lambda_{max.}^{Emis.}$, nm (solvent)	Stokes shift (nm)	Fluorescence QY, Φ_F (solvent)		
(35)	(-)	492 (PBS)	(-)	0.62[a]	ROS detection, Cell imaging; AIEgens	[66]
(36)	456, 484, 520 (MeOH)	535, 576, 625 (MeOH)	(-)	0.003 (DMSO)[b] 0.006 (MeOH) 0.16 ($CHCl_3$)	Cell imaging; Metal ion detection; monitoring of pH variations Photoinduced electron transfer (PET)	[67]

	473, 500, 535 (H_2O)	550, ~590, (H_2O)				
(37)	434 at pH 4 (H_2O) 448 at pH 11 (H_2O)	540 at pH 4 (H_2O)	99	0.47 at pH 4 (H_2O) 0.055 at pH 11 (H_2O) [c]	Cell imaging; cell death.	[68]
(38)	387 at pH 4 (H_2O) 398 at pH 11 (H_2O)	538 at pH 4 (H_2O)	145	0.50 at pH 4 (H_2O) 0.001 at pH 11 (H_2O) [c]		
(39)	433 at pH 4 (H_2O) 447 at pH 11 (H_2O)	538 at pH 4 (H_2O)	98	0.58 at pH 4 (H_2O) 0.046 at pH 11 (H_2O) [c]		
(40a)	345 (H_2O)	530 (H_2O)	185	0.03 (H_2O) [d]	Cell imaging	[70]
(40b)	416 (H_2O)	535 (H_2O)	119	0.13 (H_2O)[d]		
(41a)	520	694	174	0.06 (DMSO)	Cell imaging, cell membranes staining.	[71]
(41b)	520	(-)	(-)	0.05 (DMSO)		
(41c)	519	(-)	(-)	0.04 (DMSO)[e]		
(42a)	630 (THF)	986 (THF)	356	-	NIR imaging, latent fingerprint (LFP) imaging	[60]
(42b)	653 (THF)	-	-	-		
(42c)	637 (THF)	1098 (THF)	461	-		
(42d)	720 (THF)	-	-	-		
a: Quinine sulfate in PBS; b: Coumarin 6 (Φ_F = 0.78 in ethanol); c: Reference to disodium salt of fluorescein in ethanol (0.97); d: Quinine sulfate as reference; e: Rhodanine as reference;						

510 .

4. Oncological applications

Fluorpphores with absorption and emission in visible-NIR-FIR regions have multiple applications in oncology. For example, they can be utilized as molecular sensors for detecting various analytes, metabolic and enzymatic activities, cellular components, organelles, etc. The following sub-section highlights the utility of earlier discussed and other probes for in-vitro and in-vivo applications. Both targeted and non-targeted probes have been included in this section.

4.1. Biomedical imaging and imaging-guided therapy (Phototheranostic applications)

Recently, there has been significant attention on developing NIR emitting multimodal fluorophores for cancer diagnosis and therapy. The design and development of new theragnostic agents (probe with PDT effect and fluorescent imaging on a single unit) is an emerging trend.[73] Probe **4** (Table 1) is the first silicon xanthene-based photosensitizer with imaging capability.[36] Confocal imaging results indicated that the compound permeates into the cells and gives a strong cytosolic and nuclear signal in triple-negative breast (MDA MB-231) and colon (HCT-116) cancer cell lines. β-Gal is an important biomarker of cell senescence and primary ovarian cancer. In the quest for multi-modal probes, Shan and coworkers[74] reported a multi-modal and multi-channel probe based on a cis-amino-proline scaffold appended with different functional groups **43** (Fig. 6), which can detect specific reactive species and distinguish analytes, including enzymes. The probe showed emission from blue to red (λ_{em} = 465-640 nm) depending on the substituents. Yang et al. [19] reported a high-yielding method for synthesizing multi-modal agents (NIRF, PI, MRI and PET) based on probe **44** (Chart 1). The molecule has four sulfonic acid groups that increase its solubility. The dye, having Φ double the standard ICG, showed no quenching and photobleaching, long retention and sequestration within the tumour microenvironment. The reported probe was suitable for pre- and intraoperative procedures in cancers, including brain and breast cancers. This probe showed excellent optical properties and resisted photo-bleaching. IR-786 is a heptamethine cyanine dye with excellent optical properties and imaging capabilities. The central chloro-cyclohexene ring in such dyes forms a covalent adduct with albumin and assists in endocytosis/cellular localization.[75] Despite its mitochondrial targeting ability and photosensitizing effectiveness, its low water solubility is a major obstacle.

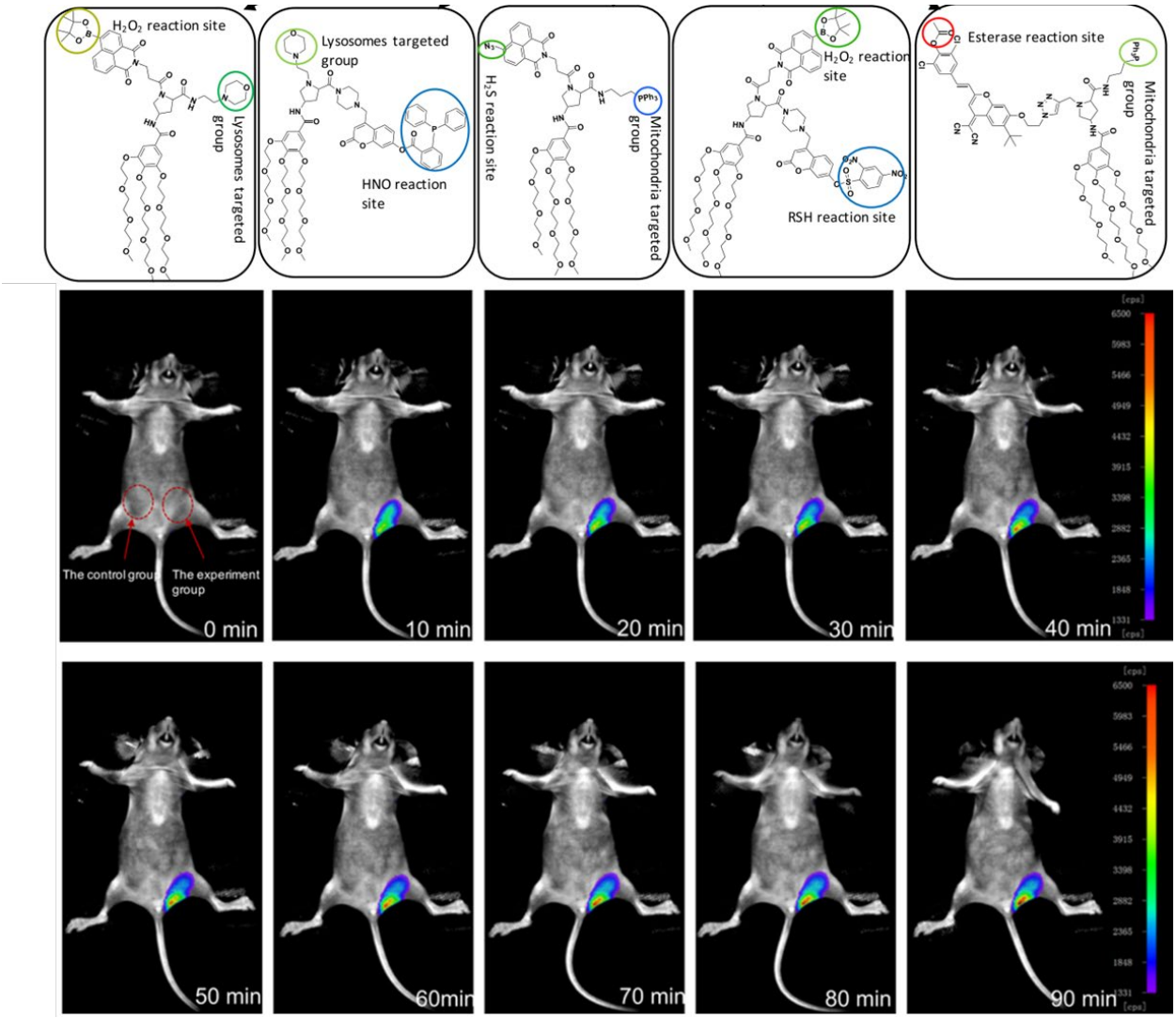

542

543 **Figure 6**: Chemical structures of 43. Fluorescence images of a nude mouse given a skin-pop
544 injection of PME (25 μL, 20 μM) in a mixture of DMSO/PBS buffer (25 mM, pH 7.4, 1:99, v/v) for
545 the control group and a subsequent skin-pop injection of esterase (25 μL, 0.5 U mL−1) in PBS
546 and PME in order. Images were taken after incubation for 0, 10, 20, 30, 40, 50, 60, 70, 80, and
547 90 min, respectively. The images were obtained with an excitation laser of 530 ± 20 nm and an
548 emission filter of 655 ± 20 nm. Reprinted with permission from Qiao D, Li L, Shen T, Yang J,
549 Chang H, Liang X, Zhang L, Wang Q, Liu N, Zhao W, Shang L., *ACS Sens*. 2020, 5, 7, 2247–
550 2254. Copyright 2020 American Chemical Society.

551 Dong and coworkers [76] reported a series of heptamethine sulfonated dyes with modified
552 central and lateral cores. They selected tyrosine amino acids to improve the water solubility and
553 fluorescence emission. In PBS, reported probes displayed $\lambda_{abs.}$ = 765-798 nm while emission
554 appeared within λ_{em} = 801-822 nm (Φ = 0.022-0.061). This was better than the standard ICG ($\lambda_{abs./}$
555 λ_{em} = 779/810 nm; Φ = 0.027) but weaker than those in organic media (DMSO). The authors used
556 probe **45** (Fig. 7) to observe lymph nodes in mice. With this probe, they were able to identify the
557 sentinel lymph node (SLN) for a period of 10-50 minutes. The results were not influenced by the

presence of dye or fat tissues. Hyun and coworkers [77] reported carboxylate IR-786 derivatives **46** and **47** (Chart 1) with improved solubility. MTT assay revealed the non-toxic nature of the compounds over a wide range of concentrations (0-20 μM on NIH/3T3 cells). IR-786 and its derivative **47** could permeate the cell and localize efficiently, indicating the importance of central chloro-cyclohexene units. Time-dependent NIR fluorescence imaging revealed that compound **47** showed excellent localization in tumors lower within 24 h post-injection, and higher tumor targetability.

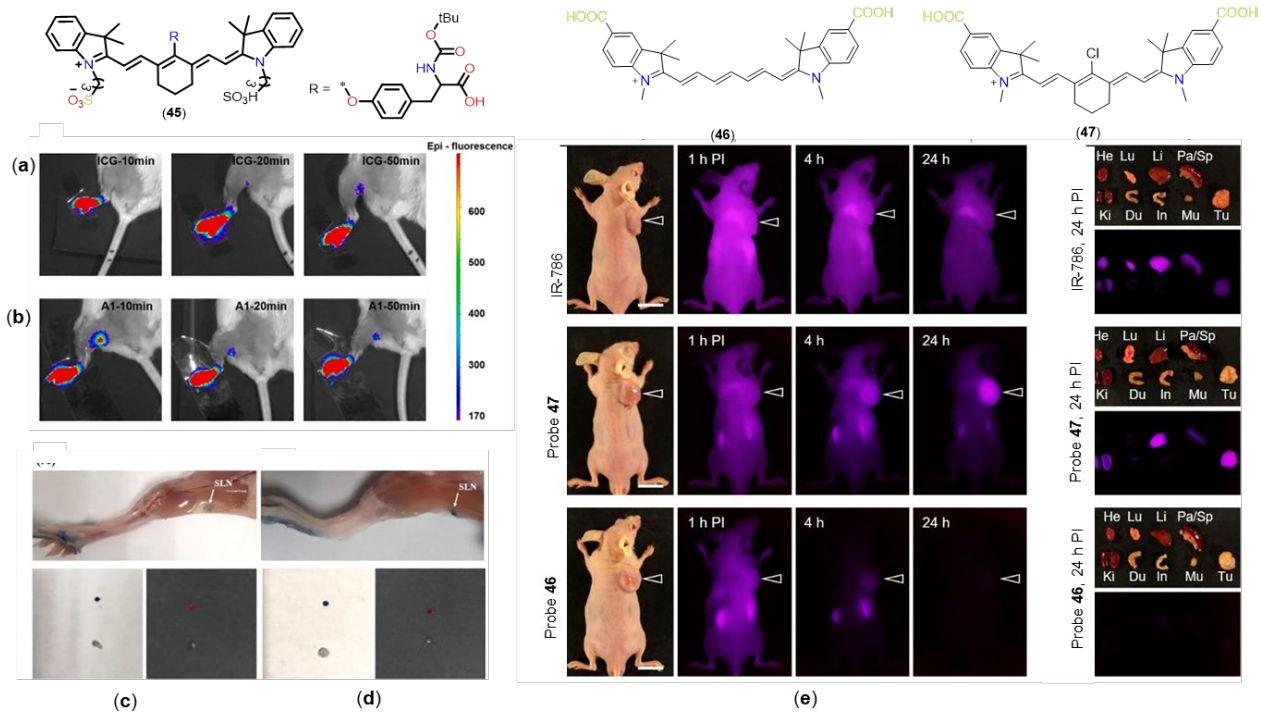

Figure 7: Chemical structures of 45-47. Visualization of lymph nodes with ICG (a) and 45 (b), in mice. Verification test of lymph node imaging (c: Color image of the mouse after blue dye injection and colour image and NIR fluorescence image of resected SLN and fat tissue using (c) 45 and ICG (d). Tumor targeting efficiency and biodistribution of NIR fluorophores 46, 47 and IR-786 (e). For further details, see original references. Reproduced with permission from ref. [76-77]

To improve the tumour targetability of a probe and use it as a multi-modal probe, Jo et al. [78] conjugated folate antagonist methotrexate to aminated ZW800-dye to obtain probe **48** (Chart 1). This probe generated photothermal energy and induced necrotic cell death of the tumour site upon photo-irradiation. Despite this, low retention time was the major drawback. The same group reported apoptotic cell death using a chlorambucil-conjugated ZW800 dye **49** (Chart 1). [79] Benefitting from the NIR emitting ability of the BODIPY core and easily functionalized B centre, **50** (Chart 1) was reported as the first example of a monomolecular cationic bimodal MRI/OI based on Wazaby. Interestingly, both ligand and Gd-complex exhibited almost similar profiles in different

solvent systems ($\lambda_{max.}^{Abs.}$ = 705 nm, $\lambda_{max.}^{Emis.}$ = 741 nm, ϕ = 10%) and was soluble in water without any surfactant. Although the probe did not produce any singlet oxygen and showed high relaxivity, no biological study was carried out.[80] Two years later, the same group reported monomolecular PET/OI compatible probe **51** (Chart 1) with red-shifted emission (734 nm) and higher Φ (15%) in water.[81] In this case, the In-complex showed relatively less Φ than the ligand in PBS. Owing to the presence of trastuzumab monoclonal antibody vector, the reported probe targeted HER-2-positive breast cancer. Radiolabelled In-complex assisted bimodal imaging (fluorescence and SPECT) and signals detected at the tumour site even after three days).

Non-covalent interactions (NCIs) are important in the materials and biological sciences, including developing bioimaging probes.[82] Very recently, Tang and co-workers [17] showed that the nature of the counterion greatly affects it property and applications. For example, **52** (Chart 1) with a bromide anion shows higher solubility than the acetate- and iodide-containing counterparts, which is attributed to the stronger hydrogen bonds between bromine ions and water. This AIE-based probe showed high water solubility, dual targetability (lysosomes + mitochondria) and resistance against photobleaching. It was suggested that the compound entered the cell through an electrostatic effect, meaning more uptake by the cancerous cells than normal, as the former possesses greater negative potential. Intratumoral injection of **52** aqueous solutions into 4T1 tumour-bearing BALB/c mice indicated that the fluorescent intensity of **52** at the tumour site was the function of time and reached the plateau after 36 h and persisted for 72 hours whereas standard dyes metabolized within 36 hrs. Nevertheless, the superior type I reactive oxygen species (ROS) produced by **52** provide both specific killings of cancer cells in vitro and inhibition of tumour growth in vivo, with negligible systemic toxicity.

It is well known that the optical properties of a D-A type conjugated system depend on various factors, including the π-conjugated spacer. Gu et al. [83] noted that imaging-guided photodynamic and photothermal therapy also depend on the π-bridge between donors and acceptors in **53a-c** (Chart 1). While **53a-b** targeted mitochondria, **53c** localized on both the cell membrane and mitochondria. Like the previous example, this probe displayed electrostatic interaction mediated penetration to the cancerous cell owing to its doubly charged character. One of the probes, **53c,** is useful for FG and PI-guided PDT and PTT and accurately locates solid tumours in mice, effectively eliminating them with good biocompatibility and biosafety to normal tissues. Probe **54** (Chart 1) is a croconaine-based D–A–D type dye with intense NIR absorption (780 nm) and fluorescence (815 nm), high photothermal conversion efficiency (77%) and generated generating hydroxyl radicals (OH) under 735 nm laser irradiation.[84] SEM results indicated that the probe

form nanoparticles in the aqueous system. Authors demonstrated that **54** ablate tumour cells by terminating DNA replication and metabolizing them by the liver and kidneys. As demonstrated earlier, switching one atom in a heterocyclic compound may cause drastic changes in the property and application of a molecule. Considering this, Xiao and coworkers[85] replaced O→S in pyrelium to realize thiopyrylium core with a lower $E_g^{op.}$ and greater NIR acceptor ability. Using this core, they prepared a series of D-A probes (instead of symmetric D-A-D type) with a feature of upconversion luminescence, i.e., fluorophores converted optical energy into heat. The water-soluble construct **55** (Chart 1) showed maximum absorption peak at ~800 nm and a maximum emission peak at ~1050 nm in water.

With BBTD as an acceptor, **56** (Chart 1) is a D-A-D type water-soluble fluorophore with an excitation peak at 738 nm and an emission at 1024 nm in an aqueous solution (Φ = 0.1%). The maxima were blue-shifted compared to the probe containing thiophene in place of EDOT. However, the one with EDOT showed greater Stoke shift (286 nm) and Φ (0.1%) than the thiophene counterpart (Stokes shift = 270 nm). It can image hind limb vasculature only after 5 mins of injection. On the other hand, the mixture of **56** with FBS showed an ability to use lymphatic system imaging within 1 min postinjection with a high spatial and temporal resolution. Upon complexation of cetuximab protein, target probes with cell-killing ability and PTT were obtained, which was helpful in colorectal cancer.[86] Shi and coworkers reported xanthene-based NIR-II dye **57** (Chart 1) by expanding π-conjugation and enhancing the intramolecular charge transfer effect.[87] The reported dyes **57c** and **57d** showed absorption extended to the NIR-II region and emission up to 1600 nm with a large Stoke shift (137-417 nm). Since the probe was non-emissive in water, the authors prepared a probe suitable for in-vivo imaging by encapsulating liposomes with DSPE-mPEG2000, which is useful for in vivo dynamic imaging of blood circulation. [87]

Chart 1: Chemical structure and photophysical data of some water-soluble probes with applications in biomedical imaging and imaging-guided therapy.

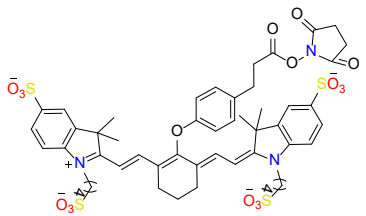

(**44**)

$\lambda_{max.}^{Abs.}$ / $\lambda_{max.}^{Emis.}$ = *774 nm/801 nm*

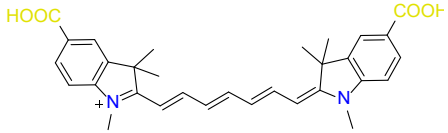

(**46**)

751 nm/776 nm

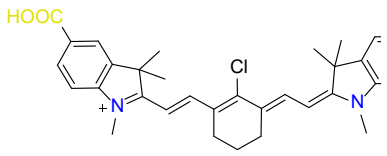

(**47**)

786/798 nm

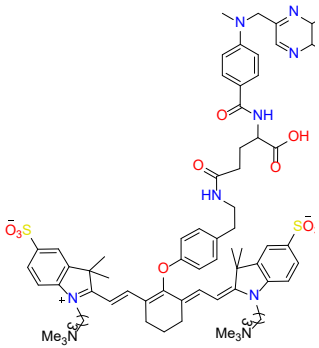

(**48**)

769/790 nm

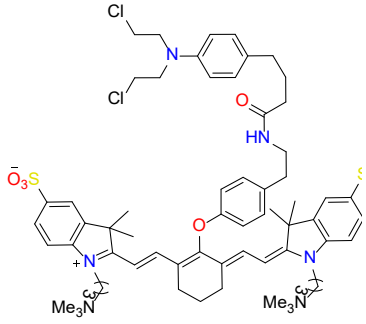

(**49**)

$\lambda_{max.}^{Abs.}$ / $\lambda_{max.}^{Emis.}$ *771 nm/793 nm*

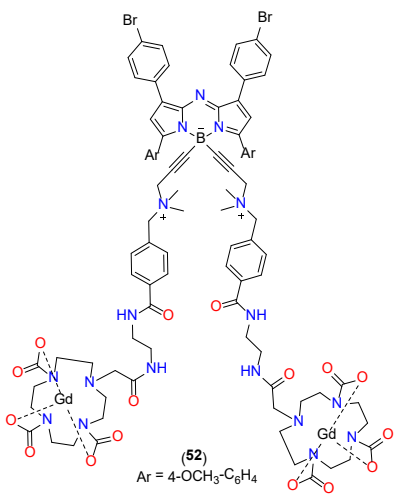

(**52**)
Ar = 4-OCH_3-C_6H_4

705 nm/741 nm

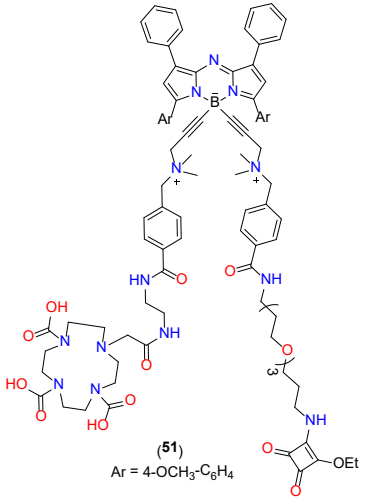

(**51**)
Ar = 4-OCH_3-C_6H_4

688 nm/734 nm

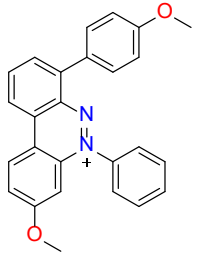

(**52**)

518 nm/732 nm

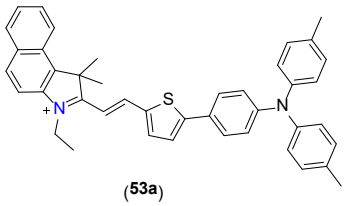

(**53a**)

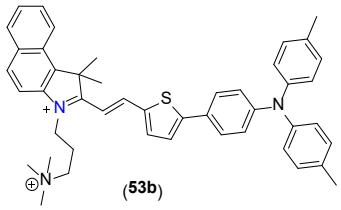

(**53b**)

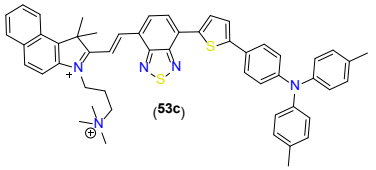

(**53c**)

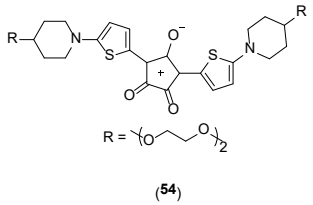

(**54**)

$\lambda_{max.}^{Abs.}$ / $\lambda_{max.}^{Emis.}$ =

620 nm/764 nm

620 nm/(-)

677 nm/938 nm

780/815 nm

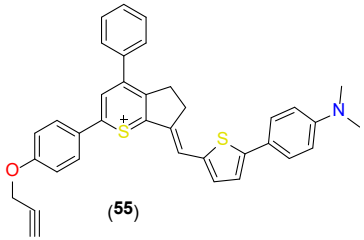

(**55**)

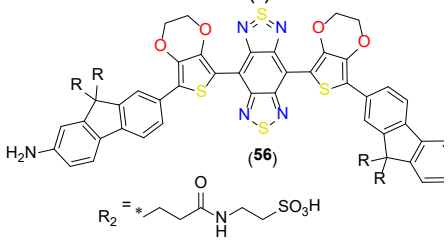

(**56**)

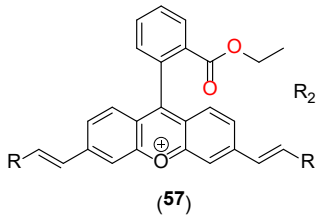

(**57**)

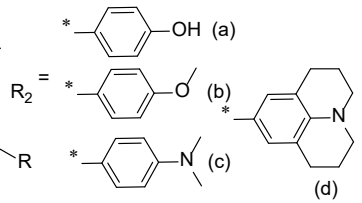

$\lambda_{max.}^{Abs.}$ / $\lambda_{max.}^{Emis.}$ =

826 nm/1100 nm

738 nm/1024 nm

670-843 nm/732-1260 nm

4.2. Analytes imaging (H_2S, CO, NO)

Following biomedical imaging and imaging-guided therapy applications of the fluorescent probes, analyte imaging in living cells is also an intriguing application. Probes emitting in visible-IR-NIR regions have shown tremendous utility in the qualitative and quantitative sensing of analytes, such as reactive species (ROS/RNS), biogenic thiols, nitric oxide, and others serving as markers for various diseases, including cancer. For example, reactive oxygen species (ROS) are mainly generated in mitochondria and responsible for physiological and pathological processes.[88] An excessive generation of ROS is the indication of abnormalities, including cardiovascular diseases, neuronal degeneration, arthritis, cancer and other diseases. [89] Therefore, a probe that can bioimage ROS with high selectivity, sensitivity, and low detection limit would be highly useful. There are various strategies to prepare a ROS-sensitive probe. For example, the high reactivity of hydrazide, thiourea, diaminomaleonitrile (DAMN), multiple bonds (C=C, C=N) and others[90] towards ROS has been utilized to prepare numerous selective probes with "*off-on*"/"*on-off*" fluorescence response. Among various types of ROS, hypochlorous acid (HClO) is produced during various physiological processes and is associated with inflammatory diseases. Probe **58** (Chart 2) is a rhodamine-based hydrazide fragment containing NIR dye for high selectivity and sensitivity towards ClO^- detection in cells and animals. Structurally, the presence of pyridine-linked PEG endowed water solubility to the compounds with mitochondrial targeting ability. It was suggested that the ROS present in the probe opened the spirolactam ring, leading to a fluorescence peak at 730 nm. MTT assay of the probe indicated the safe nature of the compounds in the range of 0–30 μM (HeLa viability > 90%) and respond in various models, including cells with oxidative stress caused by glucose, LPS-induced zebrafish and mice. Low LOD, fast response time (7 sec), high selectivity insensitivity towards divalent cations, common thiols, and other ROS/RNS make this probe highly unique.[91] Prior to this work, a probe **5** (Table 1) with a similar mechanism of action was reported by Wang and co-workers.[37] Unlike the previous example, this probe showed a change in both the absorption (increase in intensity at 603 nm) and emission (generation of the peak at 637 nm) profile upon interacting with HOCl. This probe also showed no effect of ions, amino acids, ROS/RNS, responded in 10 s with low LOD (0.9 nM), and was influential in mapping ClO^-in in-vitro and in-vivo models. This probe detected endogenous ClO^- in macrophages and targeted mitochondria due to quaternary pyridine. In very recent work, Debnath *et al*. [92] fabricated a paper-based analytical device named μPAD to detect OCl-. The device based on **59** (Chart 2) detected the analyte with very low LOD in real water samples, exogenous as well as endogenous systems. Probe **59a** was highly soluble in water with green emission (488 nm), which, upon interaction with ClO^- becomes blue (455 nm). Also, the yellow

aqueous solution became colourless, indicative of its responsiveness against ClO^-. The reported system had high selectivity and fast response (<10 s) and was able to detect OCl- in the actual water sample, exogenous as well as endogenous ClO^- in normal cells (HEK293) and cancerous cells (HeLa, Fig. 8). Leng and co-workers [93] installed DAMN core over functionalized BODIPY to obtain ClO^- sensitive probe **60** (Chart 2). This probe was able to detect ClO^- in mouse melanoma cells as well as real water sample with low cytotoxicity and appreciable detection limit (298 nM).[93] However it tool relatively longer time, the change in the optical properties was visible from the naked eyes in PBS solution. More specifically, the probe underwent a blue shift (540 to 490 nm) and an increase in the emission intensity with a little red shift (505 to 511 nm) upon the addition of ClO^-. Such shift can be attributed to breakdown of the D–π-A conjugation via ClO^- induced oxidation. The probes mentioned above have been reported to show an "*off-on*" fluorescence response based on ICT effect mechanisms. Probe **61** (Chart 2) is a "*turn on*" NIR emitting probe with high affinity towards ClO^- anion. [90] This probe also demonstrated a low detection limit (1.46 mM), fast response, can detect analytes in water sample, and animal model and worked through ICT mechanism.

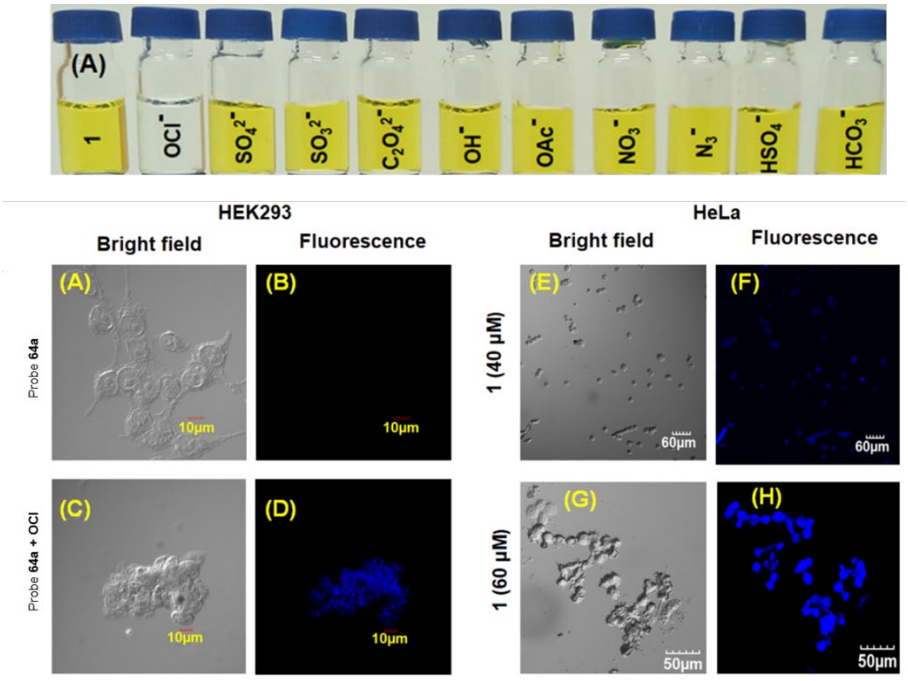

Figure 8: (Top) Response of probe **59a** towards different anions visible by the naked eye. (Bottom) Fluorescence images of **59a** HEK293 cells and HeLa cells. For exact details, see original references. Reproduced with permission from ref.[92]

Like ROS/RNS, sulfur-containing compounds are also biologically relevant, impart various effects on physiological functions and act as important biomarkers. For example, when tested against thiol and non-thiol-containing reducing species, probe **17** (Table 5) showed specificity towards cysteine, glutathione and ascorbate, indicating its utility as a fluorescent sensor for detecting reducing environment.[48] Similarly, hydrogen sulfide (H_2S) is a crucial gasotransmitter, and its elevated level has been linked to kidney, liver and cardiovascular diseases.[94] Various probes with moderate to high H_2S sensitivity via multiple mechanisms (e.g., thiolysis, nucleophilic attack, tandem Michael addition, CuS precipitation, and reduction of azide and nitro) have been reported.[95] Xu and coworkers[95] designed a highly water-soluble ratiometric probe **62** (Chart 2) that shows red-shifted emission (520 nm to 580 nm) upon the interaction with H_2S, low LOD (0.81 nM), rapid (within 10 s), and effective over a wide pH range (2.0–10.0).[95] NBD is a unique fluorescent that has been exploited to prepare several fluorescent H_2S sensors.[96] Recently, it was found that piperazine-linked rhodamine acts as a sensitive probe, which acts by thiolysis of NBD. This mitochondria-targeting probe **63** (Chart 2) displays a discernible change in the absorption and emission features. For example, the presence of H_2S enhances the emission intensity of the probe 19-fold, which NBD quenched via the PET effect. Indeed, the value was better than the structurally similar counterparts reported earlier.[96-97] A probe that can simultaneously detect and distinguish H_2S and biothiols in solution and live cells is rare.[98] Probe **64** (Chart 2) is a dual-channel fluorescent probe that can demarcate between different biothiols and target mitochondria.[99] The probe was designed so that fluorophores (coumarin and resorufin) were connected through stable but thiol-sensitive disulfide linkage (as a fluorescent unit) while NBD as the sensing unit and, therefore, two reactive sites. In the absence of analytes, probe **64** did not show any emission. However, upon the addition of H_2S or thiols, ICT perturbation and FRET removal led to the generation of blue and red emissive species. Sulphur dioxide (SO_2) is an S-based molecule that plays an important role in the permeability and fluidity of cell membranes. However, its detection remains a challenge. Probe **65** (Chart 2) is a NIR emissive probe based on diene-linked coumarin and indole sulfonate.[100] This probe showed a ratiometric behavior against SO2, targeted cells membrane, low detection limit, high selectivity, and specificity among other features.

4.3. Cellular components (plasma membrane, nuclear membrane, mitochondria, Golgi, etc.) imaging probes

A probe with excellent photophysical properties (e.g., narrow NIR ex/em band, high Φ), good water solubility, and imaging ability over an extended period hold significant promise for cancer theragnostic applications. Probes **2a,b** (Table 1) [31] are the first of its type with membrane-

targetable polarity-sensitive probes reported for cancer diagnosis. Among others, prominent features include their higher water solubility and rapid clearance time (4 hours). Like **1** (Table 1), they possess cell membrane-targeting ability without localization in the nucleus and cytoplasm region. Owing to the high Φ, probes **2a,b** illuminate the membrane at a low concentration (50 nM) within a short period (20 mins, Fig. 9). The reported probes showed superb ability to separate cancerous cells from normal ones. It is also noteworthy that fluorescent images remain the same with and without washing, indicating that a wash-free process does not affect imaging. Fluorescence imaging using **3** (Table 1) revealed that when L929 cells were incubated for 45 mins, it localized in the whole cell cytoplasm.[33] Thereby indicating good membrane permeability. It was also found to stay longer and induce low toxicity and good biocompatibility.

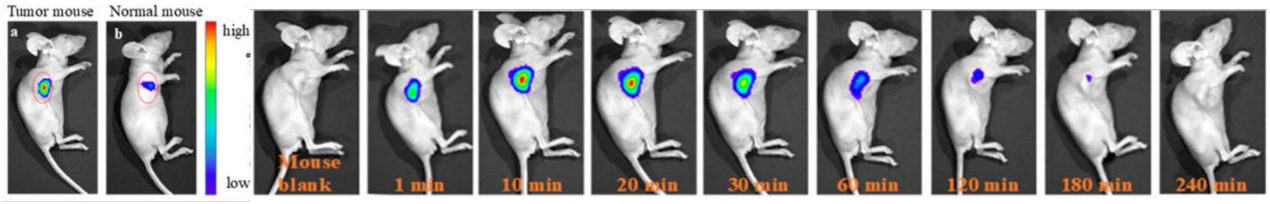

Figure 9: (a) Images of tumour-bearing mice and (b) normal mice after injection of probe **2b**. (c) Relative fluorescence intensities of mice a and b. For exact details, see original references. Reprinted with permission from Feng S, Liu Y, Li Q, Gui Z, Feng G., *Anal. Chem*. 2022, 94, 3, 1601–1607. Copyright 2022 American Chemical Society

Realizing probes that could target plasma/cell membranes is challenging. Probe **27c** (Table 6) targeted the plasma membrane exclusively.[56] The bioimaging study revealed that dye **27d** (Table 6) was mostly concentrated in the plasma membranes of the cancerous (MCF-7, A2780, T47D) and normal (HUVEC) cells in both live and fixed cells.[57]. The confocal microscopy result indicates that probe **28a** (Table 6) is mainly dispersed through the cytoplasmic region without any organelle selectivity. On the other hand, **28b** (Table 6) accumulated preferentially on the vesicles near the peripheral cell region of the cells, but a fluorescent disperses staining through all cytoplasm. However, **28c** (Table 6) showed lysosome targeting, and leakage to the cytoplasm was also noted. [58] Compounds **37** and **39a** (Table 7) were found more toxic than **38** and **39b** (**37** > **39a** > **38** > **39b**) against K562, while it was variable against MCF-7. [68]. A phase contrast study revealed apoptosis as the cell death mechanism. Fluorescence imaging data revealed nuclei and cytoplasm staining occurs in both cell lines in the presence of compound **35**.

Mitochondria is the powerhouse of the cell with membrane potential (≈ −180 mV) higher than the cell membrane and lower pH. Various charged [101] and neutral [102] dyes that could selectively target mitochondria are available in the literature. In most examples, probes with one or more

targeting moieties (such as triphenylphosphonium, pyridinium, cyanine, etc.) have been developed. There are several advantages to using two-photon imaging over one-photon imaging.Probe **40b** (Table 7) is a 2PA probe with high brightness and green to red emission spectra. [70] This probe showed lower toxicity (> 80% viability at 10 μM), and high water solubility and was localized in the mitochondria at low laser power (3.4 mW laser power). It has been reported that multiple bulky and highly polar TPP moieties are beneficial in enhancing water solubility and targeting the mitochondria. Probe **6a** (Table 2), containing charged trialkylamine, is an effective probe for imaging mitochondria in physiological environments compared to **6b** (Table 2), which exhibits ACQ.[40] As compared to the standard dye Mito Tracker Red, **6a** showed red-shifted optical properties of high ε and Φ in water. Similarly, **7b** (Table 2) was found to be excellent in imaging mitochondria than its counterpart containing three TPP units. [42] Probes **66a** and **66b** (Chart 2) are mitochondrion-targeting probes with multicolour imaging ability of the cellular organelle. These dyes exhibit excellent photostability, narrow NIR absorption and emission bands, high ε and Φ, and long lifetime.[103] Owing to the ability to show distinct excitation and emission, it was found to be helpful plasma membrane, nucleus, and mitochondria within the same cell. The same group reported found that the insertion of TPP^+ (mitochondria selective) and maleimide residue (for covalent attachment to mitochondrial through Csy) to a cyanine dye enabled a probe **67** (Chart 2) with dual localization effect and long-term live-cell mitochondrial imaging.[104] A comparative study on **26** (Table 6) and charged **27a/b** (Table 6) [56] revealed that the former disperse in the cytosol while **27a** has some preference while **27b** shows preferential localization to mitochondria. Probe **68** (Chart 2) is a polychromatic probe that showed green to NIR emission owing to different operating (AIE and TICT) mechanisms. It accumulated in lysosomes of living cells and zebrafish and generated ROS, therefore beneficial for PDT.[105]

4.4. Micro-environment (viscosity, polarity, pH sensors, enzymes) sensitive imaging probes

Changes in intracellular microenvironments viscosity, polarity, pH, and hypoxia characterize cancerous cells. Monitoring these changes is an intriguing strategy to understand cancer and develop sensitive methods for cancer diagnosis. Several studies suggest that altered lipid composition and physical properties of the cell membrane contribute to the chemoresistance of cancers.[106] One of the most common alterations in cancerous cells (especially) is the change in viscosity of the plasma membrane. A drug-resistant cancer cell is more viscous than normal with reduced drug uptake. Similarly, cancerous cells usually have negative surface charges, attracting probes with positively charged groups.[107] Probe **69** (Chart 2), a derivative of BODIPY-C_{10}, is a green-emitting water-soluble probe reported recently for staining living cell

plasma membranes.[108] A hydrophobic alkyl ($C_{12}H_{25}$) and a polar sulfonate group SO_3 allow the probe to enter the membrane swiftly. Probe **1** (Table 1) [30] is another photostable, less toxic probe that can demarcate between normal and cancerous cell membranes. This probe could stain cancerous cells in both *in-vitro* and *in-vivo* models with strong red fluorescence, indicating lower polarity than the normal cells. A probe containing azo group is usually non-fluorescent (owing to cis-trans isomerization).[109] However, upon reduction or dissociation, the fluorescent nature of the probe can restored. Using this strategy, probe **70** (Chart 2) was designed to study hypoxic conditions.[110] This probe exhibits a broad absorption (570 nm) while weak emission in PBS at physiological pH and stable over a wide pH range (3-11). When used as a hypoxic marker in HepG2 (human liver carcinoma) cells, it increased the emission intensity with time with photobleaching after 90 mins. Further, it was noted that the probe, at higher concentrations, localized within cellular nuclei, while at lower concentrations, it localized in lysosomes, Golgi apparatus, and mitochondria. Compound **16** (Table 5) is a recently reported NIR emissive and selective probe with a low detection limit, fast response, excellent cell membrane permeability, and biocompatibility [47]. It was found that the presence of LAP led to an improvement in emissions. Another enzyme that is commonly overexpressed in cancer cells is called γ-glutamyl transpeptidase (GGT). Therefore, it is important to develop an effective diagnostic tool for identifying GGT-rich cancer cells. Zhao and co-workers[59] designed a probe **71** (Chart 2) composed of a GGT recognition unit and indocyanine-BTD fluorophore, which turned on in the presence of GGT. It showed good water solubility and strong absorption band at 438 nm, which undergoes a redshift (73 nm) and hypochrmosim upon adding GGT. It was also noted that the probe had almost negligible emission at 578 nm, which was enhanced significantly upon adding GGT within a short period (25 mins).

β-galactosidase (β-Gal) is an essential biomarker of cell senescence and primary ovarian cancer. In-vivo and dynamic NIR-II imaging studies using probe **24b** (Fig. 5) revealed its multiple organ imaging capability without liposome encapsulation.[54] Successful imaging of vasculatures and organs in mice was achieved using water-soluble **24b**, which otherwise not possible with the other dyes.

Chart 2: Chemical structure and photophysical data of some water-soluble probes with applications in analytes, cellular components, and micro-environment imaging.

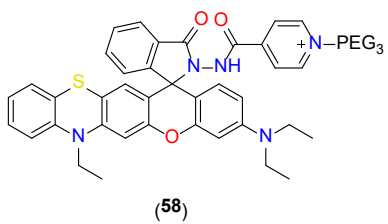

(**58**)

$\lambda_{max.}^{Abs.}$ / $\lambda_{max.}^{Emis.}$ 585 nm / 730 nm

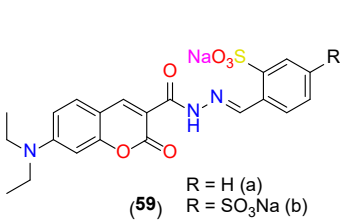

(**59**)

446/488 nm

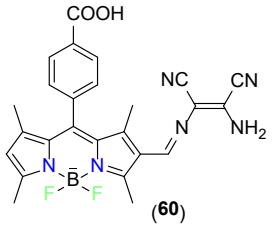

(**60**)

540/505 nm

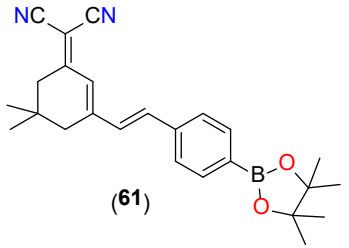

(**61**)

(-)/660 nm

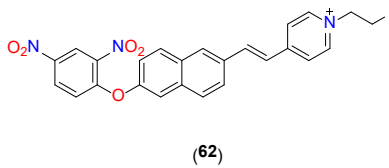

(**62**)

$\lambda_{max.}^{Abs.}$ / $\lambda_{max.}^{Emis.}$ 370 nm/520 nm

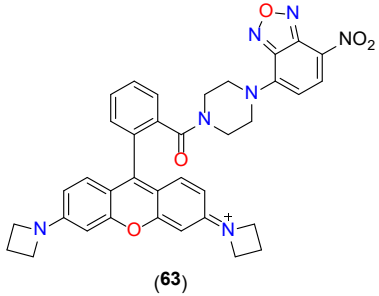

(**63**)

502/530 nm

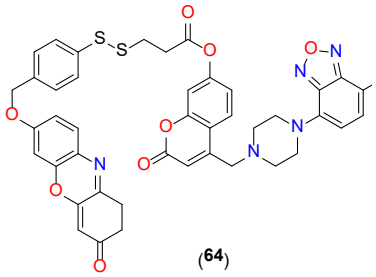

(**64**)

475 nm/467 and 588 nm

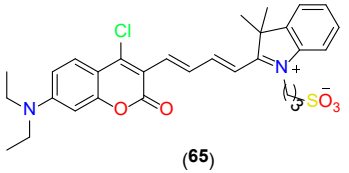

(**65**)

580 nm/720 nm

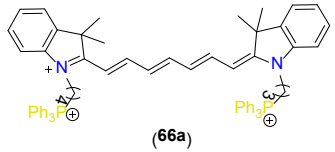

(**66a**)

$\lambda_{max.}^{Abs.}$ / $\lambda_{max.}^{Emis.}$ 644/663nm

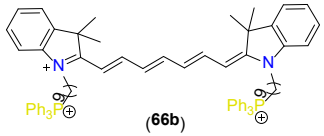

(**66b**)

645/663 nm

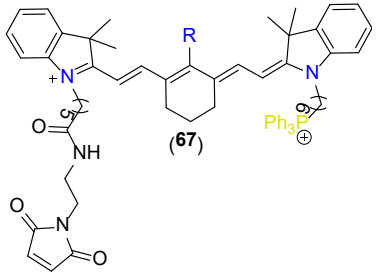

(**67**)

644/664 nm

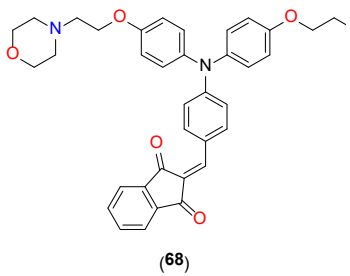

(**68**)

500 nm/ 677 nm

827

	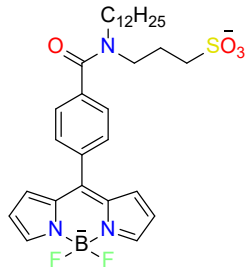	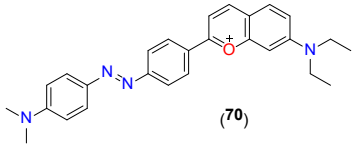	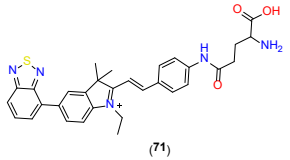
	(**69**)	(**70**)	(**71**)
$\lambda_{max.}^{Abs.}$ / $\lambda_{max.}^{Emis.}$	503/523 nm	570/(-)	438/578 nm

4.5. Prodrug delivery (visible or near-infrared light-triggered photocages)

An exciting and emerging application of a fluorescent probe is to develop a photoactivated probe that can release bioactive molecules in subcellular locations using light.[111] Such probes, also known as photoremovable protecting groups (PPG), photocages, or photoactivatable or photocleavable groups, mask the substrates (leaving groups, LG such as carboxylic acids, phenols etc.) through covalent linkage. However, upon irradiation with suitable light, the leaving group is cleaved, releasing and restoring their function and activity. In this context, recently, PPGs based on coumarin, BODIPY, cyanine frames, and metal complexes have been investigated. Although PPGs with excitation wavelength in the UV-Vis region are known to have varying photolysis efficiency, the success of photoprotecting/ photocaging/ groups significantly depends on their water solubility. Among several examples of PPGs, BODIPY-based ones are pretty interesting as they offer tunable PL properties and solubility. Weinstain and coworkers [112] found that introducing an electron-withdrawing group (e.g. sulphonate) at 2,6 position of BODIPY reduces its photocaging ability, attributed to the destabilization of carbocation formed during the photoreaction. A remote/peripheral sulfonation strategy that served solubility and photorelease ability was suggested to overcome this issue. Depending upon the number of sulphonated groups (**72-73**, Chart 3), PPGs show cellular interaction (Fig. 10).

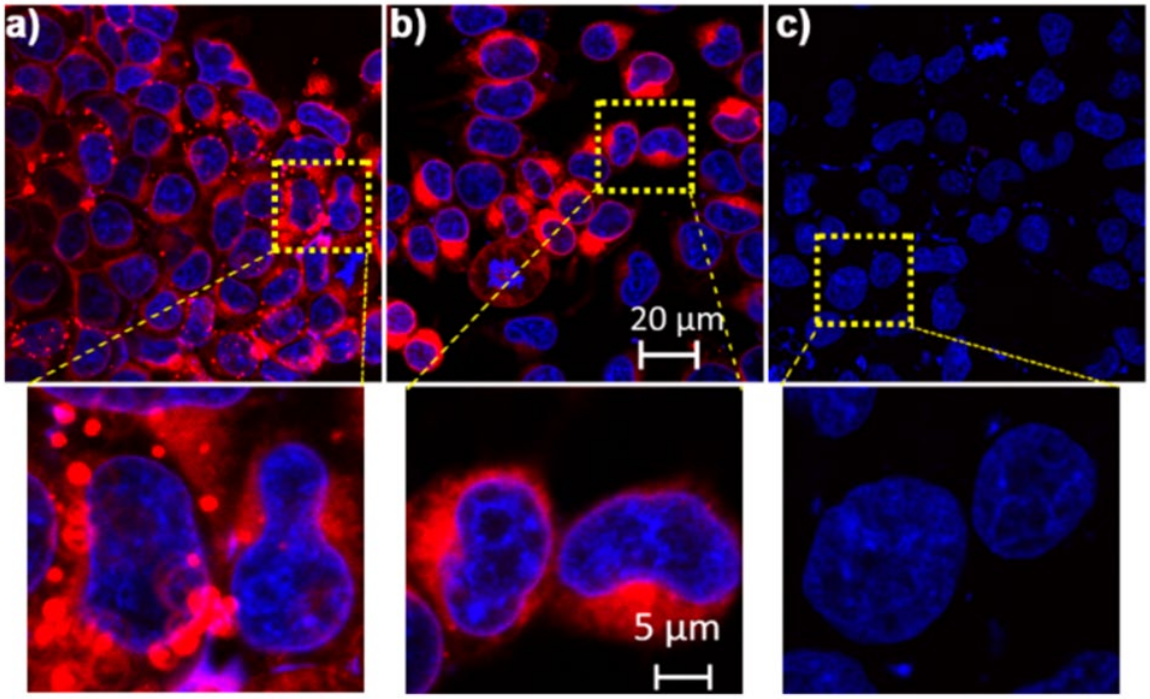

Figure 10: Confocal fluorescence microscopy of HEK 293T cells treated with BODIPY **72**, **73a**, or **73b** (2 µM) for 30 min and costained with Hoechst dye. Reproduced with permission from ref. [112] under CC-BY-NC-ND.

Recently, coumarin-based photocages known as COUPY **74** & **75** (Chart 3) were reported with absorption between 557-570 nm and emission maxima between 619-634 nm (Φ = 0.06-0.1).[113] In such probes, the caging/uncaging process using yellow and red light in PBS was the function of core caging (coumarin) and the leaving groups. It was noted that the electron-donating alkyl group next to the photocleavable bond is a key parameter for modulating the photoactivation process. Prior to this work, Li and co-wokers [114] reported **76** (Chart 3) with good cell-membrane permeability and bioavailability that release blue/NIR light-triggered halogen (Cl, Br) atoms. Kele and coworkers [115] reported green, orange, or red light-triggered carboxanthenium derivatives **77** & **78** (Chart 3) as water-soluble photocages for the delivery of anticancer drugs. The probes showed absorption in the 538-643 nm range while emission between 564-676 nm in H_2O/ACN at physiological pH.

Chart 3: Chemical structure and photophysical data of some water-soluble probes with visible or near-infrared light-triggered photocages.

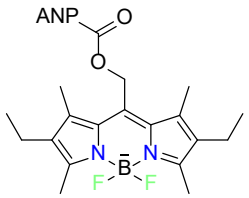

(**72**)

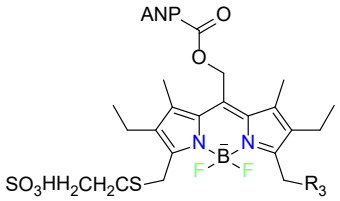

(**73**)
R = H (a)
R = $S(CH_2)_2SO_3H$ (b)

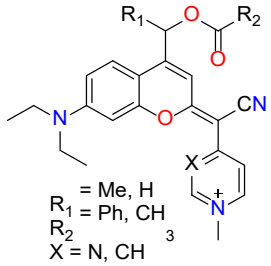

(**74**)

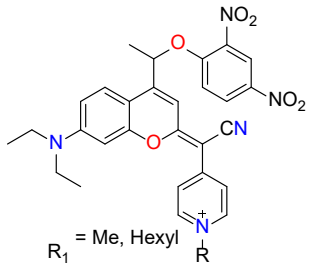

(**75**)

$\lambda_{max.}^{Abs.}$ / $\lambda_{max.}^{Emis.}$ 556 nm/564 nm

545/570-577

555-570 nm/619-634 nm

560-563/613-619

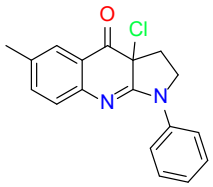

(**76a**)

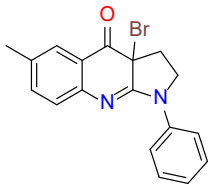

(**76b**)

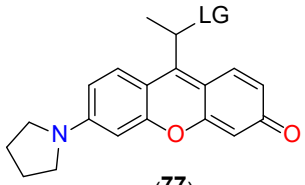

(**77**)

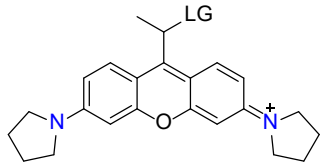

(**78**)

$\lambda_{max.}^{Abs.}$ / $\lambda_{max.}^{Emis.}$ 442/580

455/610

538/564 nm

570/592 nm

5. Future perspectives

Design and development of new OI probes with absorption/emission encompassing visible-NIR regions, high brightness, and stability are highly demanding as they offer multiple features and broad-ranging applications. If the probe is soluble in water, its value is greatly enhanced. Indeed, a water-soluble organic probe offers benefits over other fluorescent systems (such as nano) in terms of ease of access, reproducibility, functionalization and toxicity. They are promising alternatives to the existing arduous techniques related to bioimaging. In the present scenario, several organic dyes are commercially available and used in clinical settings. With the advent of modern instrumentation and super-resolution fluorescence microscopy, one may globally or precisely image/map the changes at the sub-cellular level in a real-time manner. It is now possible to synthesize new molecules with high-resolution imaging capability using state-of-the-art technologies.

Similarly, judicious functionalization using a bio-recognition unit endows selective uptake of the dye. Besides, without compromising the absorption/emission profile, the multi-modal probe that can home in tumour cells for days can also be realized for practical applications. As we have highlighted, a single probe offers multi-channel detection and can be used for imaging-guided therapy and surgery. In addition to the discussed examples of water-soluble fluorescent dyes with therapeutic/diagnostic applications of cancer, several other interesting probes with membrane potential imaging,[116] microbial imaging[117], Tau fibrils imaging[118], anti-biofilm[119], metal ion detection[120], hydrazine detection[121] etc. also exist. Some probes have also shown enhanced emission properties by forming inclusion complexes.[122] Other probes with applications in ureter visualization[123], kidney damage[124], Cu(II) ion[120], monoamine oxidase (MAO) [125], reducing environment [48], BSA[126]., etc. have also been the subject of study.

However, benefits always come up with some challenges. For example, π-conjugated organic fluorophores, owing to their hydrophobic nature, suffer from poor water solubility. While installation of a polar functionality is mainly adopted to circumvent the problem of poor solubility, it has been noted that the incorporation of conventional ionic substituents hydrophilicity-lipophilicity balance.[18b] As evidenced by several studies, π-π interaction in such probes has a deleterious effect on the optical properties of the probe. In some cases, limited photo-stability and off-target cellular accumulation hinder its application. It is also known that the benzyl chloride group present in Mito Tracker dyes is responsible for the cytotoxicity.[127] While probes emitting in the NIR-II region are highly promising for various in-vivo applications, a water soluble core with enough brightness is rare. In many cases, the use of high concentrations of organic solvents (>10%, v/v) can cause significant harm to living organisms. Probes that are converted to nano-

formulation are metabolized through hepatobiliary pathways, which can result in long-term toxicity. Besides, lack of imaging instruments suitable for such probes is also a problem. Multi-step synthesis, low yield, and harsh storage conditions are also matters of concern,. Various interesting probes are available for the detection of bio-analytes. However, many feature *turn-on* responses with a single detection region sensitive to the cellular environment.

As we highlighted using pertinent examples, researchers utilize techniques such as late-stage functionalization to improve water solubility. Strategies such as one-atom replacement have emerged as a unique strategy to achieve a new generation of promising dyes. For example, replacing one atom (O → C) of rhodamine scaffolds produces carborhodamine, while replacing B → C in BODIPYs yields CARBOPYs. Some other classes of molecules that require the attention of the scientific community are oligo-ynes and metalla-ynes. Several interesting new works related to the bioimaging application of oligo-ynes have been demonstrated. Various researchers demonstrated that the luminescence features of this class of materials could be combined with water solubility to realize probes suitable for cellular and microorganism imaging.[128] For instance, the use of alkyne-tagged small precursors for the imaging of DNA. RNA, protein, phospholipids and other biomolecules. We also believe that the ionic liquid appended probes hold promise for such application owing to the balanced solubility profile, green synthesis, compatibility and stability.

6. Conclusion

To qualify as a promising probe for application in oncology, a molecule/system with improved physicochemical properties, enhanced contrast, long circulation and tumour retention time, and clinical translation ability are required. In recent years, tremendous progress has been made in designing and developing water-soluble fluorescent organic probes. Numerous probes with potential applications in bioimaging and analyte detections in living cells have been reported with excellent water solubility and stability towards chemical, photo-bleaching, and others. Besides, they maintain their brightness after incubation in cellular environments, which makes it highly useful for defect analyses and progress.

Acknowledgement

This research has been funded by Scientific Research Deanship at University of Ha'il-Saudi Arabia through project number MDR-22 006.

Conflict of interest statement

On behalf of all authors, the corresponding author states that there is no conflict of interest.

References

1. Sung H, Ferlay J, Siegel RL, Laversanne M, Soerjomataram I, Jemal A, Bray F (2021) CA Cancer J Clin 71: 209. doi:10.3322/caac.21660
2. Ward ZJ, Scott AM, Hricak H, Atun R (2021) Lancet Oncol 22: 341. doi:10.1016/S1470-2045(20)30750-6
3. Brandon D, Alazraki A, Halkar RK, Alazraki NP (2011) Seminars in oncology, vol 38. Elsevier p 87
4. Shokrollahi H (2013) Mater Sci Eng C Mater Biol Appl 33: 4485. doi:10.1016/j.msec.2013.07.012
5. Seemann MD (2005) Technol Cancer Res Treat 4: 577. doi:10.1177/153303460500400512
6. Murar M, Albertazzi L, Pujals S (2022) Nanomaterials (Basel) 12: 399. doi:10.3390/nano12030399
7. Yang K, Zhang S, He J, Nie Z (2021) Nano Today 36: 101046.
8. Louie A (2010) Chem Rev 110: 3146. doi:10.1021/cr9003538
9. aGeorgiev NI, Bakov VV, Anichina KK, Bojinov VB (2023) Pharmaceuticals 16: 381. ; bLi X, Gao X, Shi W, Ma H (2014) Chem Rev 114: 590. doi:10.1021/cr300508p; cZhu C, Liu L, Yang Q, Lv F, Wang S (2012) Chemical reviews 112: 4687. ; dXu Z, Xu L (2016) Chem Commun (Camb) 52: 1094. doi:10.1039/c5cc09248e; eNeto BA, Corrêa JR, Silva RG (2013) RSC advances 3: 5291. ; fXu W, Wang D, Tang BZ (2021) Angewandte Chemie International Edition 60: 7476. ; gZhou L, Lv F, Liu L, Wang S (2019) Accounts of Chemical Research 52: 3211.
10. Fan G, Yang L, Chen Z (2014) Frontiers of Chemical Science and Engineering 8: 405.
11. Zhu C, Liu L, Yang Q, Lv F, Wang S (2012) Chem Rev 112: 4687. doi:10.1021/cr200263w
12. Sun H, Schanze KS (2022) ACS Appl Mater Interfaces 14: 20506. doi:10.1021/acsami.2c02475
13. Stegemann S, Leveiller F, Franchi D, De Jong H, Lindén H (2007) European journal of pharmaceutical sciences 31: 249.
14. Hill AP, Young RJ (2010) Drug Discov Today 15: 648. doi:10.1016/j.drudis.2010.05.016
15. aBisballe N, Laursen BW (2020) Chemistry–A European Journal 26: 15969. ; bSun M, Mullen K, Yin M (2016) Chem Soc Rev 45: 1513. doi:10.1039/c5cs00754b; cShi Z, Han X, Hu W, Bai H, Peng B, Ji L, Fan Q, Li L, Huang W (2020) Chem Soc Rev 49: 7533. doi:10.1039/d0cs00234h
16. Maillard J, Klehs K, Rumble C, Vauthey E, Heilemann M, Fürstenberg A (2021) Chemical Science 12: 1352.
17. Liu L, Li C, Gong J, Zhang Y, Ji W, Feng L, Jiang G, Wang J, Tang BZ (2023) Angew Chem Int Ed Engl 62: e202307776. doi:10.1002/anie.202307776
18. aKohl C, Weil T, Qu J, Mullen K (2004) Chemistry 10: 5297. doi:10.1002/chem.200400291; bYanai H, Hoshikawa S, Moriiwa Y, Shoji A, Yanagida A, Matsumoto T (2021) Angew Chem Int Ed Engl 60: 5168. doi:10.1002/anie.202012764
19. Yang J, Zhao C, Lim J, Zhao L, Tourneau RL, Zhang Q, Dobson D, Joshi S, Pang J, Zhang X, Pal S, Andreou C, Zhang H, Kircher MF, Schmitthenner H (2021) Theranostics 11: 2534. doi:10.7150/thno.54928
20. Wang A, Ma Y, Zhou L, Lu S, Lin Y, Zhou J, Wei S (2013) Dyes and Pigments 99: 348.

21. aWais U, Jackson AW, He T, Zhang H (2016) Nanoscale 8: 1746. doi:10.1039/c5nr07161e; bGrossi M, Morgunova M, Cheung S, Scholz D, Conroy E, Terrile M, Panarella A, Simpson JC, Gallagher WM, O'Shea DF (2016) Nat Commun 7: 10855. doi:10.1038/ncomms10855
22. Pliquett J, Dubois A, Racoeur C, Mabrouk N, Amor S, Lescure R, Bettaieb A, Collin B, Bernhard C, Denat F, Bellaye PS, Paul C, Bodio E, Goze C (2019) Bioconjug Chem 30: 1061. doi:10.1021/acs.bioconjchem.8b00795
23. Bardon KM, Selfridge S, Adams DS, Minns RA, Pawle R, Adams TC, Takiff L (2018) ACS Omega 3: 13195. doi:10.1021/acsomega.8b01487
24. Godard A, Kalot G, Pliquett J, Busser B, Le Guevel X, Wegner KD, Resch-Genger U, Rousselin Y, Coll JL, Denat F, Bodio E, Goze C, Sancey L (2020) Bioconjug Chem 31: 1088. doi:10.1021/acs.bioconjchem.0c00175
25. Hughes LD, Rawle RJ, Boxer SG (2014) PloS one 9: e87649.
26. Chang Z, Liu F, Wang L, Deng M, Zhou C, Sun Q, Chu J (2019) Chinese Chemical Letters 30: 1856.
27. Dsouza RN, Pischel U, Nau WM (2011) Chemical reviews 111: 7941.
28. aKaraman O, Alkan GA, Kizilenis C, Akgul CC, Gunbas G (2023) Coordination Chemistry Reviews 475: 214841. ; bCao D, Liu Z, Verwilst P, Koo S, Jangjili P, Kim JS, Lin W (2019) Chemical reviews 119: 10403.
29. Wodarz A, Näthke I (2007) Nature cell biology 9: 1016.
30. Li Q, Hong J, Feng S, Gong S, Feng G (2022) Anal Chem 94: 11089. doi:10.1021/acs.analchem.2c02312
31. Feng S, Liu Y, Li Q, Gui Z, Feng G (2022) Analytical Chemistry 94: 1601.
32. Sun YQ, Liu J, Lv X, Liu Y, Zhao Y, Guo W (2012) Angewandte Chemie (International ed. in English) 51: 7634.
33. Jiao X, Liu C, Huang K, Zhang S, He S, Zhao L, Zeng X (2015) Org Biomol Chem 13: 6647. doi:10.1039/c5ob00448a
34. Egawa T, Koide Y, Hanaoka K, Komatsu T, Terai T, Nagano T (2011) Chemical Communications 47: 4162.
35. Zhao M, Guo Y-S, Xu W-N, Zhao Y-F, Xie H-Y, Li H-J, Chen X-F, Zhao R-S, Guo D-S (2020) TrAC Trends in Analytical Chemistry 122: 115704.
36. Cetin S, Elmazoglu Z, Karaman O, Gunduz H, Gunbas G, Kolemen S (2021) ACS Med Chem Lett 12: 752. doi:10.1021/acsmedchemlett.1c00018
37. Wang TR, Zhang XF, Huang XQ, Cao XQ, Shen SL (2021) Spectrochim Acta A Mol Biomol Spectrosc 247: 119115. doi:10.1016/j.saa.2020.119115
38. Wang Z, Li X, Sun X, Zhang X, He C, Li Y, Lu F, Lu X, Fan Q (2023) Sensors and Actuators B: Chemical 384: 133627.
39. Benniston AC, Copley G (2009) Phys Chem Chem Phys 11: 4124. doi:10.1039/b901383k
40. Wang J-L, Zhang L, Gao L-X, Chen J-L, Zhou T, Liu Y, Jiang F-L (2021) Journal of Materials Chemistry B 9: 8639.
41. Sutter A, Elhabiri M, Ulrich G (2018) Chemistry 24: 11119. doi:10.1002/chem.201801540
42. Mai DK, Badon IW, Lim JM, Vales TP, Kim C, Yang J, Lee J, Kim H-J (2022) Dyes and Pigments 208: 110856.
43. Godard A, Kalot G, Privat M, Bendellaa M, Busser B, Wegner KD, Denat F, Le Guevel X, Coll JL, Paul C, Bodio E, Goze C, Sancey L (2023) J Med Chem 66: 5185. doi:10.1021/acs.jmedchem.3c00100
44. Zhang H, Liu J, Sun Y-Q, Liu M, Guo W (2020) Journal of the American Chemical Society 142: 17069.
45. Gopika G, Prasad PH, Lekshmi A, Lekshmypriya S, Sreesaila S, Arunima C, Kumar MS, Anil A, Sreekumar A, Pillai ZS (2021) Materials Today: Proceedings 46: 3102.

46. Chai Y, Gao Y, Xiong H, Lv W, Yang G, Lu C, Nie J, Ma C, Chen Z, Ren J, Wang F (2019) Analyst 144: 463. doi:10.1039/c8an01486h
47. Tao L, Liu S, Xia X, Chai Y, Cai S, Liu H, Lu C, Ma C, Nie J, Zeng F (2021) Tetrahedron 99: 132449.
48. Heing-Becker I, Achazi K, Haag R, Licha K (2022) Dyes and Pigments 201: 110198.
49. Cai X, Zhang J, Ye H, Cui K, Hao T, Yi L, Yang X (2023) Chemistry–A European Journal: e202301105.
50. Zhang K, Zhang J, Xi Z, Li L-Y, Gu X, Zhang Q-Z, Yi L (2017) Chemical science 8: 2776.
51. Li DH, Gamage RS, Oliver AG, Patel NL, Muhammad Usama S, Kalen JD, Schnermann MJ, Smith BD (2023) Angew Chem Int Ed Engl 62: e202305062. doi:10.1002/anie.202305062
52. Li B, Lu L, Zhao M, Lei Z, Zhang F (2018) Angewandte Chemie 130: 7605.
53. Meador WE, Autry SA, Bessetti RN, Gayton JN, Flynt AS, Hammer NI, Delcamp JH (2020) J Org Chem 85: 4089. doi:10.1021/acs.joc.9b03108
54. Zhang X, Shen S, Liu D, Li X, Shi W, Ma H (2023) Chemical Science 14: 2928.
55. Neto BA, Correa JR, Spencer J (2022) Chemistry–A European Journal 28: e202103262.
56. Carvalho PH, Correa JR, Paiva KL, Baril M, Machado DF, Scholten JD, de Souza PE, Veiga-Souza FH, Spencer J, Neto BA (2019) Organic Chemistry Frontiers 6: 2371.
57. Carvalho P, Correa JR, Paiva KLR, Machado DFS, Scholten JD, Neto BAD (2019) Beilstein J Org Chem 15: 2644. doi:10.3762/bjoc.15.257
58. Souza VS, Corrêa JR, Carvalho PH, Zanotto GM, Matiello GI, Guido BC, Gatto CC, Ebeling G, Goncalves PF, Dupont J (2020) Sensors and Actuators B: Chemical 321: 128530.
59. Guo S, Zhu T, Wang R, Gao J, Sun J, Ou-Yang Z, Liu Y, Gu X, Zhao C (2022) Bioorg Med Chem Lett 68: 128762. doi:10.1016/j.bmcl.2022.128762
60. He K, Chen S, Chen Y, Li J, Sun P, Lu X, Fan Q, Huang W (2021) ACS Applied Polymer Materials 3: 3238.
61. Liu C, Wang X, Zhu X, Ma R, Lin Q, Liang Y (2023) Materials Chemistry Frontiers 7: 2419.
62. Li Q, Ding Q, Li Y, Zeng X, Liu Y, Lu S, Zhou H, Wang X, Wu J, Meng X, Deng Z, Xiao Y (2020) Chem Commun (Camb) 56: 3289. doi:10.1039/c9cc09865h
63. Sun Y, Ding M, Zeng X, Xiao Y, Wu H, Zhou H, Ding B, Qu C, Hou W, Er-Bu A, Zhang Y, Cheng Z, Hong X (2017) Chem Sci 8: 3489. doi:10.1039/c7sc00251c
64. Shi W, Diao S, Liang T, Zhang X, Guo Z, Liu Y, Zhou W, Xie C, Fan Q (2022) ACS Appl Bio Mater 5: 4965. doi:10.1021/acsabm.2c00682
65. Xu C, Zou H, Zhao Z, Zhang P, Kwok RT, Lam JW, Sung HH, Williams ID, Tang BZ (2019) Advanced Functional Materials 29: 1903278.
66. Pan D, Don Y, Lu Y, Xiao G, Chi H, Hu Z (2022) Anal Chim Acta 1235: 340559. doi:10.1016/j.aca.2022.340559
67. Georgiev NI, Said AI, Toshkova RA, Tzoneva RD, Bojinov VB (2019) Dyes and Pigments 160: 28.
68. Johnson AD, Zammit R, Vella J, Valentino M, Buhagiar JA, Magri DC (2019) Bioorganic Chemistry 93: 103287.
69. Ohshita J (2009) Macromolecular Chemistry and Physics 210: 1360.
70. Auvray M, Bolze F, Clavier G, Mahuteau-Betzer F (2021) Dyes and Pigments 187: 109083.
71. Rzewnicka A, Krysiak J, Pawlowska R, Zurawinski R (2023) Materials (Basel) 16: 1806. doi:10.3390/ma16051806
72. Rzewnicka A, Krysiak J, Pawlowska R, Zurawinski R (2023) Int J Mol Sci 24: 9620. doi:10.3390/ijms24119620
73. Wen Y, Schreiber CL, Smith BD (2020) Bioconjugate Chemistry 31: 474.

74. Qiao D, Li L, Shen T, Yang J, Chang H, Liang X, Zhang L, Wang Q, Liu N, Zhao W, Shang L (2020) ACS Sens 5: 2247. doi:10.1021/acssensors.0c00992
75. Usama SM, Park GK, Nomura S, Baek Y, Choi HS, Burgess K (2020) Bioconjug Chem 31: 248. doi:10.1021/acs.bioconjchem.9b00771
76. Zhang S, Ji X, Zhang R, Zhao W, Dong X (2022) Bioorg Med Chem Lett 73: 128910. doi:10.1016/j.bmcl.2022.128910
77. Lim W, Byun JY, Jo G, Kim EJ, Park MH, Hyun H (2022) Pharmaceutics 14: 676. doi:10.3390/pharmaceutics14030676
78. Jo G, Kim EJ, Park MH, Hyun H (2022) Int J Mol Sci 23: 14127. doi:10.3390/ijms232214127
79. Jo G, Kim EJ, Hyun H (2022) Int J Mol Sci 23: 14093. doi:10.3390/ijms232214093
80. Florès O, Pliquett J, Abad Galan L, Lescure R, Denat F, Maury O, Pallier A, Bellaye P-S, Collin B, Même S (2020) Inorganic Chemistry 59: 1306.
81. Privat M, Bellaye PS, Lescure R, Massot A, Baffroy O, Moreau M, Racoeur C, Marcion G, Denat F, Bettaieb A, Collin B, Bodio E, Paul C, Goze C (2021) J Med Chem 64: 11063. doi:10.1021/acs.jmedchem.1c00450
82. Wang J, Gu X, Zhang P, Huang X, Zheng X, Chen M, Feng H, Kwok RT, Lam JW, Tang BZ (2017) Journal of the American Chemical Society 139: 16974.
83. Gu H, Liu W, Sun W, Du J, Fan J, Peng X (2022) Chem Sci 13: 9719. doi:10.1039/d2sc02879d
84. Pang E, Huang R, Zhao S, Yang K, Li B, Tan Q, Tan S, Lan M, Wang B, Song X (2022) J Mater Chem B 10: 9848. doi:10.1039/d2tb01772e
85. Zhou H, Zeng X, Li A, Zhou W, Tang L, Hu W, Fan Q, Meng X, Deng H, Duan L, Li Y, Deng Z, Hong X, Xiao Y (2020) Nat Commun 11: 6183. doi:10.1038/s41467-020-19945-w
86. Zeng X, Xiao Y, Lin J, Li S, Zhou H, Nong J, Xu G, Wang H, Xu F, Wu J, Deng Z, Hong X (2018) Adv Healthc Mater 7: e1800589. doi:10.1002/adhm.201800589
87. Liu D, He Z, Zhao Y, Yang Y, Shi W, Li X, Ma H (2021) J Am Chem Soc 143: 17136. doi:10.1021/jacs.1c07711
88. Checa J, Aran JM (2020) J Inflamm Res 13: 1057. doi:10.2147/JIR.S275595
89. Debnath S, Ghosh R, Nair RR, Pradhan D, Chatterjee PB (2022) ACS Omega 7: 38122. doi:10.1021/acsomega.2c04840
90. Zhen L, Lan J, Zhang S, Liu L, Zeng R, Chen Y, Ding Y (2022) Anal Methods 14: 2147. doi:10.1039/d2ay00561a
91. He M, Ye M, Li B, Wu T, Lu C, Liu P, Li H, Zhou X, Wang Y, Liang T (2022) Sensors and Actuators B: Chemical 364: 131868.
92. Debnath S, Ghosh R, Pragti, Mukhopadhyay S, Baskaran KV, Chatterjee PB (2023) Analyst 148: 4072. doi:10.1039/d3an00533j
93. Leng J, Nie W, Yuan L, Liu S, Liu T, Cheng J, Liu Z (2022) ChemistrySelect 7: e202200378.
94. Stein A, Bailey SM (2013) Redox Biol 1: 32. doi:10.1016/j.redox.2012.11.006
95. Guo FF, Han XF, Zhao XL, Wang Y, Fan YC, Wu WN, Xu ZH (2022) Spectrochim Acta A Mol Biomol Spectrosc 270: 120835. doi:10.1016/j.saa.2021.120835
96. Wang R, Li Z, Zhang C, Li Y, Xu G, Zhang QZ, Li LY, Yi L, Xi Z (2016) ChemBioChem 17: 962.
97. Ismail I, Wang D, Wang D, Niu C, Huang H, Yi L, Xi Z (2019) Org Biomol Chem 17: 3389. doi:10.1039/c8ob03219j
98. aLiu J, Sun Y-Q, Zhang H, Huo Y, Shi Y, Guo W (2014) Chemical Science 5: 3183. ; bDai X, Wang ZY, Du ZF, Cui J, Miao JY, Zhao BX (2015) Anal Chim Acta 900: 103. doi:10.1016/j.aca.2015.10.023

99. Qiao D, Shen T, Zhu M, Liang X, Zhang L, Yin Z, Wang B, Shang L (2018) Chemical Communications 54: 13252.
100. Liu T, Zhao W, Guo Z, Zhai Y, Zhang W, Yang X, Chen D, Yin C (2022) Sensors and Actuators B: Chemical 368: 132098.
101. Yaqoob MD, Xu L, Li C, Leong MML, Xu DD (2022) Photodiagnosis Photodyn Ther 38: 102830. doi:10.1016/j.pdpdt.2022.102830
102. Kesavan PE, Pandey V, Raza MK, Mori S, Gupta I (2019) Bioorg Chem 91: 103139. doi:10.1016/j.bioorg.2019.103139
103. Saha PC, Chatterjee T, Pattanayak R, Das RS, Mukherjee A, Bhattacharyya M, Guha S (2019) ACS Omega 4: 14579. doi:10.1021/acsomega.9b01890
104. Saha PC, Das RS, Das S, Sepay N, Chatterjee T, Mukherjee A, Bera T, Kar S, Bhattacharyya M, Sengupta A, Guha S (2023) Bioconjug Chem 34: 1407. doi:10.1021/acs.bioconjchem.3c00185
105. Dai Y, He F, Ji H, Zhao X, Misal S, Qi Z (2020) ACS Sens 5: 225. doi:10.1021/acssensors.9b02090
106. Kopecka J, Trouillas P, Gasparovic AC, Gazzano E, Assaraf YG, Riganti C (2020) Drug Resist Updat 49: 100670. doi:10.1016/j.drup.2019.100670
107. Bu Y, Xu T, Zhu X, Zhang J, Wang L, Yu Z, Yu J, Wang A, Tian Y, Zhou H, Xie Y (2020) Chem Sci 11: 10279. doi:10.1039/d0sc03093g
108. Polita A, Stancikaite M, Zvirblis R, Maleckaite K, Dodonova-Vaitkuniene J, Tumkevicius S, Shivabalan AP, Valincius G (2023) RSC Adv 13: 19257. doi:10.1039/d3ra04126c
109. Kiyose K, Hanaoka K, Oushiki D, Nakamura T, Kajimura M, Suematsu M, Nishimatsu H, Yamane T, Terai T, Hirata Y, Nagano T (2010) J Am Chem Soc 132: 15846. doi:10.1021/ja105937q
110. Pewklang T, Wet-Osot S, Wangngae S, Ngivprom U, Chansaenpak K, Duangkamol C, Lai RY, Noisa P, Sukwattanasinitt M, Kamkaew A (2021) Molecules 26: 4938. doi:10.3390/molecules26164938
111. Shrestha P, Kand D, Weinstain R, Winter AH (2023) J Am Chem Soc 145: 17497. doi:10.1021/jacs.3c01682
112. Kand D, Liu P, Navarro MX, Fischer LJ, Rousso-Noori L, Friedmann-Morvinski D, Winter AH, Miller EW, Weinstain R (2020) J Am Chem Soc 142: 4970. doi:10.1021/jacs.9b13219
113. López-Corrales M, Rovira A, Gandioso A, Nonell S, Bosch M, Marchán V (2023) The Journal of Organic Chemistry.
114. Situ Z, Chen W, Yang S, Fan X, Liu F, Wong NK, Dang L, Phillips DL, Li MD (2022) J Phys Chem B 126: 3338. doi:10.1021/acs.jpcb.2c01440
115. Egyed A, Németh K, Molnár TÁ, Kállay M, Kele P, Bojtár M (2023) Journal of the American Chemical Society 145: 4026.
116. Franke JM, Raliski BK, Boggess SC, Natesan DV, Koretsky ET, Zhang P, Kulkarni RU, Deal PE, Miller EW (2019) J Am Chem Soc 141: 12824. doi:10.1021/jacs.9b05912
117. Singh S, Meador WE, Pramanik A, Ray P, Delcamp JH, Zhao Y (2023) J Photochem Photobiol B 240: 112652. doi:10.1016/j.jphotobiol.2023.112652
118. Ji L, Zhou X, Liu R, Wang L, Hu Y, Gu J, Li Z, Li C, Huang T, Yu Y (2023) Sensors and Actuators B: Chemical 380: 133415.
119. Manna SK, Chakraborty S, Adak AK, Samanta S (2022) ChemistrySelect 7: e202200729.
120. Wang X, Li Z, Nie J, Wu L, Chen W, Qi S, Xu H, Du J, Shan Y, Yang Q (2021) RSC Adv 11: 10264. doi:10.1039/d0ra09894a
121. Jin Y, Sun R, Li G, Yuan M, Shao W, Cao M, Yuan C, Wang S (2023) Spectrochim Acta A Mol Biomol Spectrosc 294: 122558. doi:10.1016/j.saa.2023.122558
122. Ayhan MM, Özcan E, Alkan F, Çetin M, Ün I, Bardelang D, Çoşut B (2022) Materials Advances 3: 547.

123. Cha J, Nani RR, Luciano MP, Kline G, Broch A, Kim K, Namgoong JM, Kulkarni RA, Meier JL, Kim P, Schnermann MJ (2018) Bioorg Med Chem Lett 28: 2741. doi:10.1016/j.bmcl.2018.02.040
124. Zeng C, Tan Y, Sun L, Long Y, Zeng F, Wu S (2023) ACS Appl Mater Interfaces 15: 17664. doi:10.1021/acsami.3c00956
125. Shang J, Shi W, Li X, Ma H (2021) Anal Chem 93: 4285. doi:10.1021/acs.analchem.0c05283
126. Tu Y, Yu Y, Zhou Z, Xie S, Yao B, Guan S, Situ B, Liu Y, Kwok RTK, Lam JWY, Chen S, Huang X, Zeng Z, Tang BZ (2019) ACS Appl Mater Interfaces 11: 29619. doi:10.1021/acsami.9b10359
127. Cottet-Rousselle C, Ronot X, Leverve X, Mayol JF (2011) Cytometry A 79: 405. doi:10.1002/cyto.a.21061
128. aYamakoshi H, Dodo K, Palonpon A, Ando J, Fujita K, Kawata S, Sodeoka M (2012) J Am Chem Soc 134: 20681. doi:10.1021/ja308529n; bLi S, Chen T, Wang Y, Liu L, Lv F, Li Z, Huang Y, Schanze KS, Wang S (2017) Angew Chem Int Ed Engl 56: 13455. doi:10.1002/anie.201707042; cLiu L, Wong WY, Shi JX, Cheah KW (2006) Journal of Polymer Science Part A: Polymer Chemistry 44: 5588. doi:10.1002/pola.21666; dGupta V, Carroll KS (2016) Chem Sci 7: 400. doi:10.1039/C5SC02569A